AN ABSTRACT OF THE THESIS OF

Stanley Francis Wasowski (Name) for the Master of Science (Degree)

in Oceanography (Degree) presented on September 6, 1973 (Date)

Title: MEASUREMENTS OF TURBULENT VELOCITIES AND AN EXAMINATION OF THEIR EFFECTS ON MIXING AND SUSPENSION OF PARTICULATE MATTER

Redacted for privacy

Abstract approved: Dr. H. Pak

An experiment was conducted in which a three component drag probe was used to measure the three directional components of turbulent velocity. While velocity measurements were being made, water samples were taken and analyzed for salinity and suspended particulate matter. Three dimensional energy spectra were computed from the velocity records between .1 and 5 Hz. These were compared with theoretical values. In the wave-number ranges corresponding to the inertial subrange the spectra showed good agreement with the -5/3 power law. Reynolds stress tensors were computed. The norms of the Reynolds' stresses were used in a multilinear Regression model for particulate matter concentration and vertical variability of particulate matter concentrations. Although crude, the models

accounted for over 60 percent of the variability in measured concentrations and over half the variability in vertical coefficient of variation.

Measurements of Turbulent Velocities and an Examination of Their Effects on Mixing and Suspension of Particulate Matter

by

Stanley Francis Wasowski, Jr.

A THESIS

submitted to

Oregon State University

in partial fulfillment of
the requirements for the
degree of

Master of Science

June 1974

APPROVED:

Redacted for privacy

Research Associate in Oceanography
in charge of major

Redacted for privacy

Dean, School of Oceanography

Redacted for privacy

Dean of Graduate School

Date thesis is presented September 6, 1973

Typed by Cheryl E. Curb for Stanley Francis Wasowski, Jr.

ACKNOWLEDGEMENTS

I am deeply indebted to Dr. Ha Song Pak under whom I carried out this research. I wish to thank Drs. Clayton Paulson and Joel Davis for their helpful discussions and suggestions. I am grateful to Dr. D. H. Carlson and Mr. S. Corder who served on my committee.

A word of thanks to my parents for their interest and encouragement and especially to my wife, Kathleen, whose constant support was invaluable during my research.

This work was supported by the Office of Naval Research under contract N00014-67-A-0369-0007.

TABLE OF CONTENTS

Chapter		Page
I.	INTRODUCTION	1
II.	BACKGROUND	4
III.	INSTRUMENTATION	16
	The Drag Probe	17
	Calibration	19
	Modifications	20
IV.	THE EXPERIMENT	22
V.	HANDLING OF SAMPLES AND DATA PROCESSING	26
	Water Samples	26
	Drag Probe Records	29
VI.	DISCUSSION	35
VII.	CONCLUSIONS	60
	BIBLIOGRAPHY	63
	APPENDICES	65
	Appendix 1	65
	Appendix 2	68
	Appendix 3	85
	Appendix 4	88

MEASUREMENTS OF TURBULENT VELOCITIES AND AN EXAMINATION OF THEIR EFFECTS ON MIXING AND SUSPENSION OF PARTICULATE MATTER

I. INTRODUCTION

The problem of mixing in a tidal estuary is a complex one, full of variables and interactions. Knowledge of these mixing characteristics, however, is useful and may, at times, be crucial if we are to use these areas without destroying them as a natural resource. With the demands of an increasing population, a tidal estuary comes under pressure from many interests seeking its utilization. Surrounding communities, as well as those up river, must obtain water and dispose of sewage. Industry needs to dispose of waste and heat as well as take in raw materials. The list is long. Whether the tidal estuary can survive depends in a large part on how well the physical parameters which affect it are understood and to what extent this understanding is implemented in the planned use of the areas' resources. One important factor is the effectiveness with which the estuary can mix the incoming contaminants with sea water and flush them into the ocean. What happens then is still another problem.

Since turbulent diffusion is so much more effective at mixing than molecular diffusion, it is appropriate that the turbulence in the area of interest be investigated. The interaction of turbulence with the various characteristics of fluid flow has been the subject of much

research. Due to the non-linearity of the Navier-Stokes equation of motion when applied to turbulent flows, a closed solution, even with very simple boundary conditions, is virtually impossible. In view of this difficulty, many attempts have been made to describe turbulent flows through the use of simplifying assumptions as well as using statistical techniques. The most widely used approach is to divide the flow into mean and fluctuating parts, to describe the fluctuations statistically, and to relate the statistics to products of coefficients and properties of the mean flow. Evaluation of these coefficients is determined through experimentation, dimensional analysis, or similarity theory.

A primary difficulty in taking turbulence measurements in the oceanic environment has been the lack of a suitable sensor. Earle (1971) describes many sensor types and their various strengths and weaknesses for use in measuring salt water turbulent flows. The sensor developed by Earle and later modified by this author is the one which was used in the experiment which will be described in this thesis.

The purpose of the experiment was twofold. First is to use the modified three component drag probe to obtain measurements of the turbulent velocity field. Since all three components of velocity would be measured, it would be possible to obtain a more direct evaluation of the three-dimensional spectral density function E(k). Grant, Stewart and Moilliet (1961) stated that, "No way is known by

which E(k) may be measured directly." They went on to say that the usual experimental method employed was to make measurements of the one-dimensional spectrum and relate it to the three-dimensional spectral density function assuming isotropy. In addition to E(k), other parameters could be calculated directly if the three components of velocity were known. Among these would be the Reynolds' Stress tensor τ_{ij}. These parameters could then be compared with the predictions for them based on theory.

The second purpose is to measure the amount of particulate matter in the water column and its distribution. With this data and the data from the turbulence measurements it was hoped that some light could be shed on the effect of turbulence on mixing in a tidal estuary.

II. BACKGROUND

Some factors which affect the process of mixing in a tidal estuary are the geographical configuration of the estuary, the submarine topography, the volume of the tidal prism, the volume of the fresh water runoff, and the mixing which occurs outside the estuary. A brief discussion of these factors is in order before the experiment itself is presented.

Since there is no such thing as a typical tidal estuary, consider for a moment a highly idealized model to explore the effects on the dynamics of varying some of the parameters of the model.

In response to the tides in the ocean, the water level in the estuary changes. On an incoming tide, water flows into the estuary from the ocean and the water level rises. On an outgoing tide, the water flows out of the estuary into the ocean and the water level falls. While this is happening fresh water from the river is continually flowing to the estuary. The ocean water is salty, hence denser than the fresh river water.

To get a more quantitative picture of the dynamics, a model estuary is constructed. Figures 1 and 2 show a plan and side view of the estuary. The dimensions are as follows: length 10^4 meters, width 10^3 meters, depth 10 meters. Outside the estuary, the tide ranges 1 meter above and 1 meter below mean sea level. The tidal

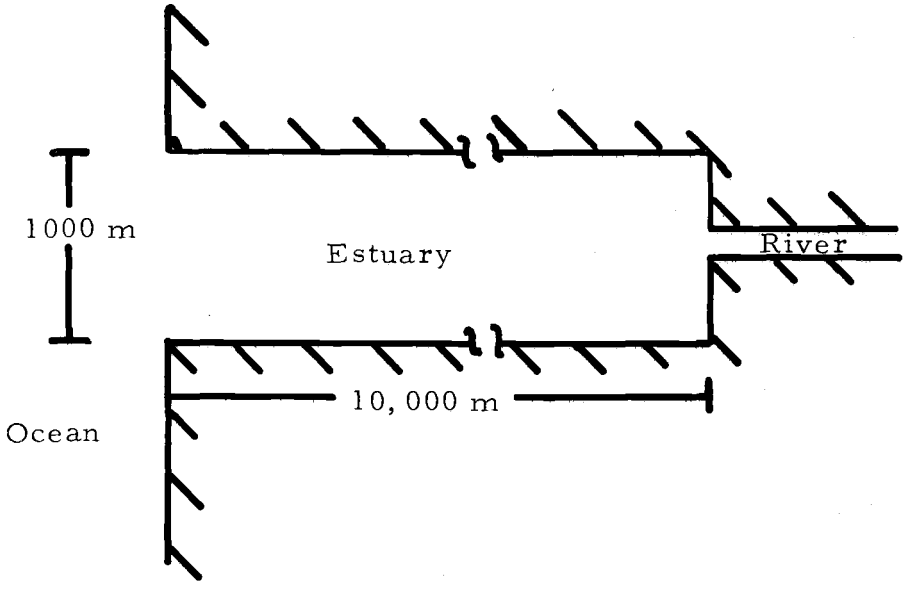

Figure 1. Model estuary, plan view.

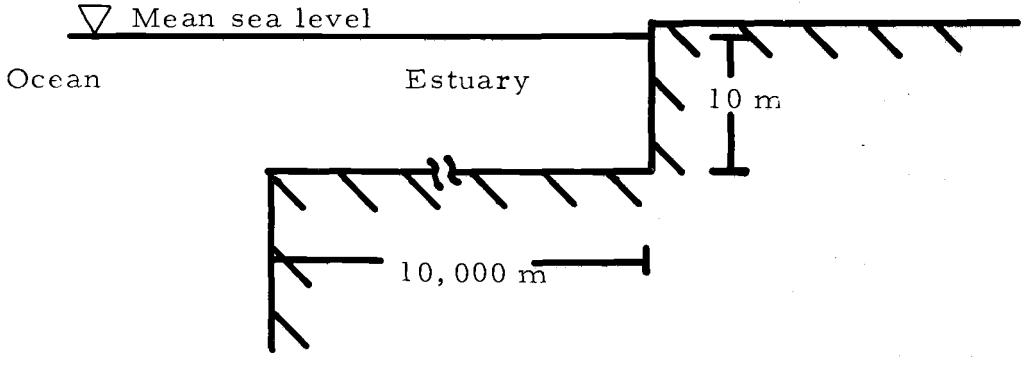

Figure 2. Model estuary, side view.

period is 5×10^4 sec. approximately 14 hours. If the tide is considered a wave, equations which describe its behavior are:

$$c^2 = \frac{g}{k} \tanh (kh) \tag{1}$$

and

$$\eta = 2a \sin (k(1-x)) \cos (\sigma T) \tag{2}$$

where c = the celerity of the traveling wave form

L = wavelength

T = wave period

k = wave number $2n/L$

h = water depth

η = water surface elevation

a = wave amplitude

σ = wave frequency $2n/T$

t = time

x = distance from inland end of estuary

l = length of estuary

Using these equations, the waveform of the tide inside the estuary can be calculated. Under the above conditions, the surface profiles of the wave at high and low tides are given in Figure 3.

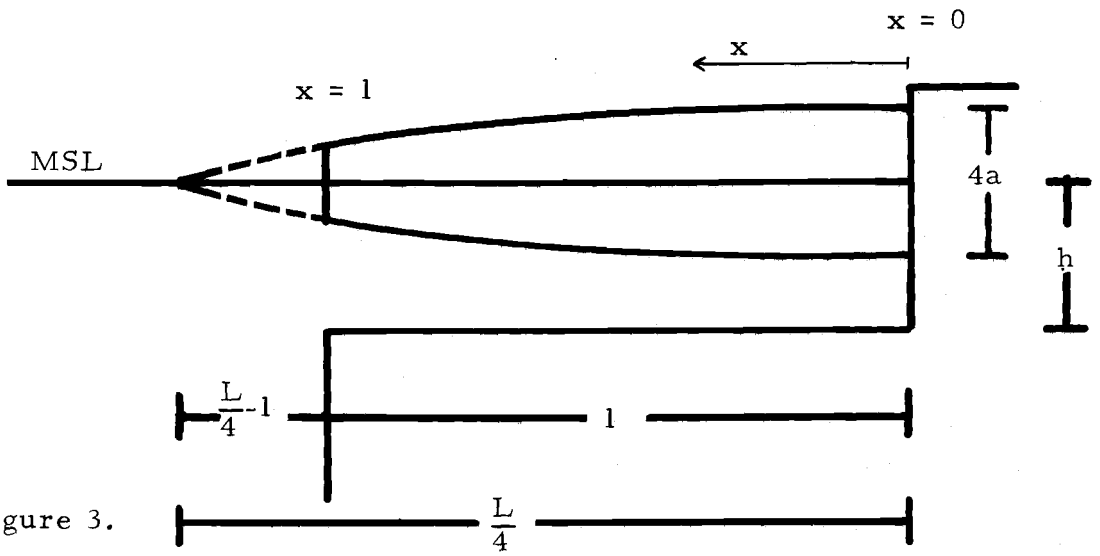

Figure 3.

The volume between the surface at high tide and that at low tide is equal to the tidal prism. In this case it is 2×10^7 m^3. The ratio of the volume of fresh water which flows into the estuary during a tidal period to the tidal prism is a parameter which is often used to classify estuaries. If the constant river is 20m wide and 10m deep, flowing at an average speed of 90 cm/sec, the volume of fresh water which will flow into the estuary during a tidal period will be 8×10^6 m^3. The ratio of fresh to salt water is 1:4. This ratio is well within the range found in nature: for example, the Mississippi River estuary has a high fresh water outflow coupled with the relatively low Gulf coast tides giving it a ratio of 1:1. On the other hand, the Delaware Bay estuary has a lower fresh water runoff and the higher Atlantic coast tidal range to give a ratio of about 1:100 (Ippen, 1966). When this ratio of fresh to salt water is used as an indicator, estuaries are

usually divided into three categories: highly stratified, where the ratio is unity or greater, partly mixed, where the ratio is .8 to .2, and well mixed, where the ratio is 0.1 or less (Ippen, 1966). The model estuary as described above is partly mixed. Salt water forces its way below the less dense fresh water when responding to the force of an incoming tide. The result is called a saline wedge shown in Figure 4. A plot of the motion of a saline wedge over a tidal period results in a pattern very much like that in Figure 5. Besides the motion of the wedge as a whole, there is a circulation within the wedge which is set up by the shear forces at the fresh-salt water interface. As a result of the circulation, in both high stratified and partly mixed estuaries, there is a net transport of water upstream at or below a certain depth within the wedge. Above this depth there is net flow downstream which usually increases as one approaches the surface (Ippen, 1966). Figure 6 shows the relative transport for incoming and outgoing tides near the bottom at mid-depth and near the surface for each of the described types. Unfortunately, this classification of estuaries is neither definitive nor time independent. An estuary with a fresh to salt water ratio consistent with a partly mixed classification may in fact be well mixed due to the particular flow configuration or other factors. One which is partly mixed or highly stratified during periods of high rainfall may become well mixed during dryer periods. This latter condition is typical of many estuaries in Oregon.

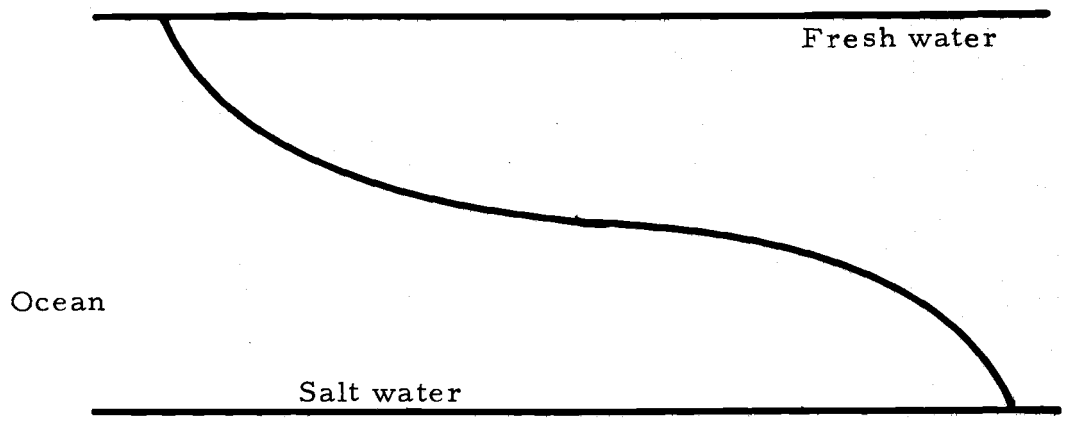

Figure 4. Saline wedge, side view.

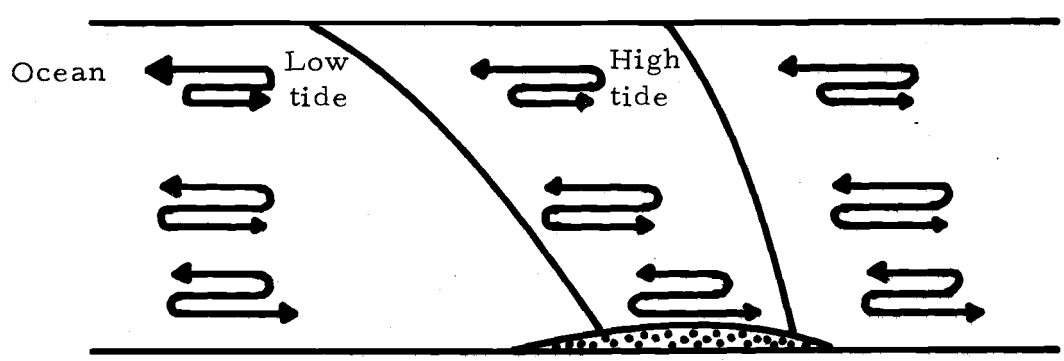

Figure 5. Motion of saline wedge.

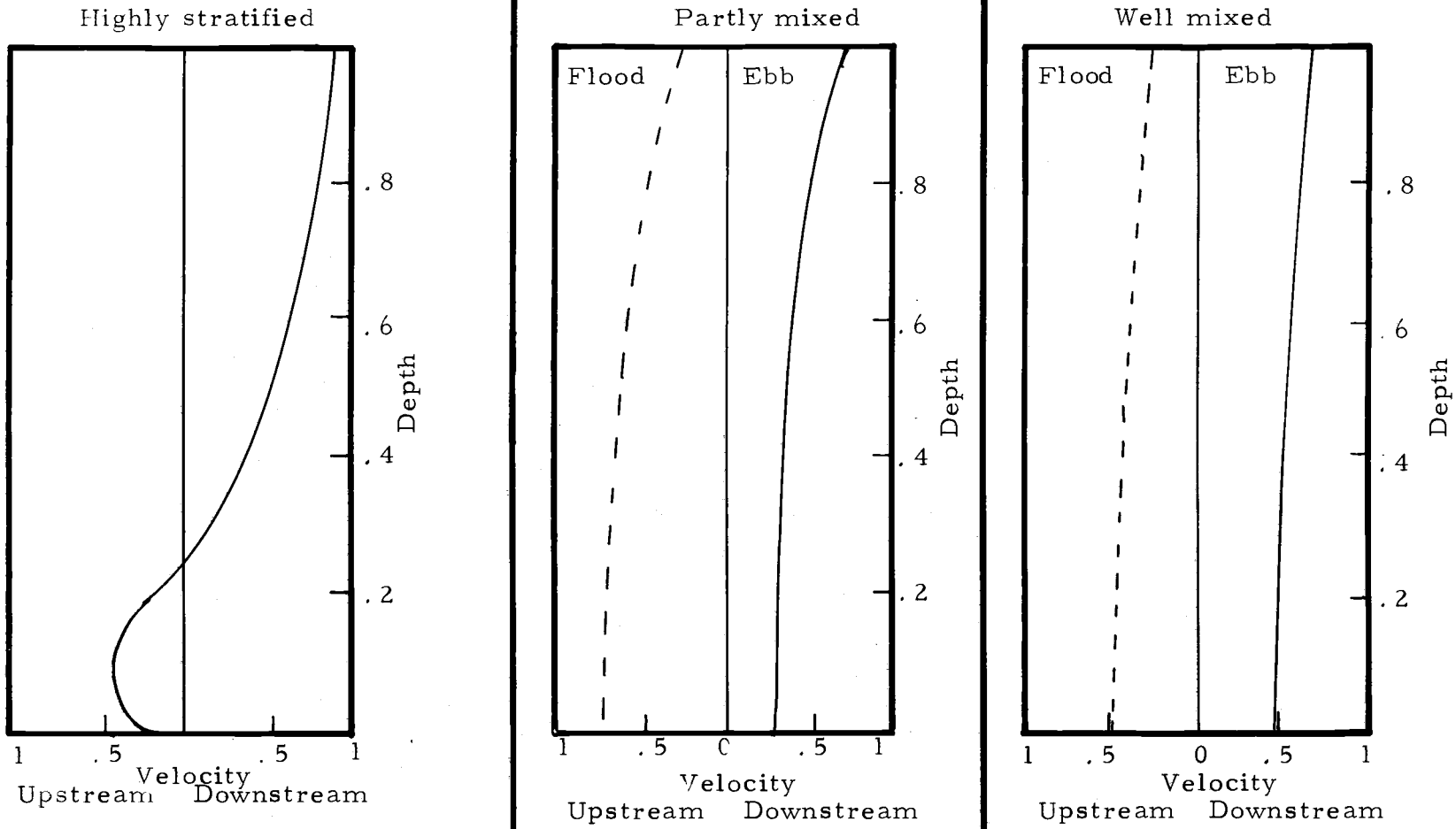

Figure 6. Relative transport.

The amount of salt water which flows into the estuary is determined primarily by the tidal range and by the geography of the area. In the highly simplified model it is merely the surface area of the estuary times the tidal range; however, in most real estuaries the lateral boundaries are not vertical nor are they straight. This greatly complicates the determination of the tidal prism. In addition the tidal range is not usually constant and, in fact, may vary greatly between spring and neap tides. Besides affecting the volume of the tidal prism, the geography of the area affects the way the estuary fills and drains during a tidal period. Because the lateral boundaries of the model estuary were normal to the coastline, it was somewhat justifiable to examine a two-dimensional model of the circulation pattern. As soon as complications are introduced into the boundaries, the two-dimensional model no longer represents the actual dynamics of the system. To illustrate, examine the effects of a few simple changes in the geography of the model estuary. The model had a tidal prism of 2×10^7 m^3 and a tidal period of 5×10^4 sec. A volume of water equal to the tidal prism must be transferred into and out of the estuary during each tidal period. A mean velocity may then be calculated at the mouth of the estuary. Dividing the volume per unit time by the area of the opening of the estuary to the ocean gives a mean velocity for the transfer. In the case of the model the mean velocity is equal to 4 cm/sec. The results can be very different if the tidal prism and

the area remain the same but the shape of the estuary changes. Applying the same analysis as above to estuaries of the shapes given in Figure 7 the results are as follows:

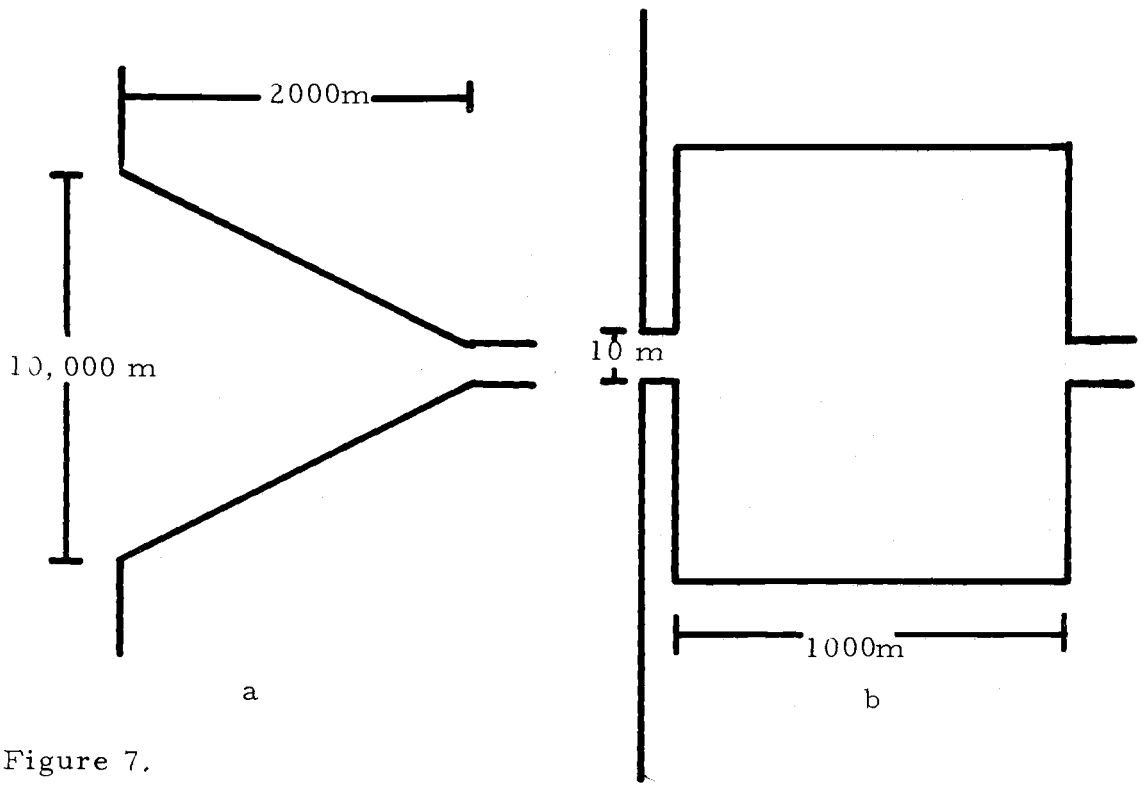

Figure 7.

Since the volume flux of water remains the same, the only factor which will affect the mean velocity will be the area of the opening to the sea. In Figure 7a this is 10^5 m^2, resulting in a velocity of 4×10^{-1} cm/sec. In Figure 7b the area is 10^2 m^2, which results in a velocity of 400 cm/sec. The geographical configuration of the inlet therefore can alter the velocity of the tidal current over several orders of magnitude. Examples of these types of situations are the Delaware Bay and San Francisco Bay estuaries, respectively.

The boundaries in the vertical plane can exert as much influence on the dynamics of estuarine flow as those in the horizontal plane. The model estuary has a flat bottom which allows us to calculate rather easily the shape of the tide within the basin. The flow patterns can then be derived from wave theory. If bottom topography is allowed, the flow patterns are uncertain. The basic considerations are similar to those for horizontal variations in the boundary; however, the vertical dimension in most estuaries is an order of magnitude or smaller than either of the horizontal dimensions, and the effects of irregularities are proportionately amplified. In addition to large scale inhomogeneities such as bars, the very composition of the bottom can substantially affect the vertical flow characteristics. Whether the bottom is composed of silts and clays or large rocks influences the roughness factor which can in turn affect the intensity of the mixing.

The volume of material which can be transported depends on the volume of water transported and on the concentration. The volume of water transported may be divided into tidal and non-tidal volume transport. The volume of the tidal prism determines the amount of tidal volume available for flushing. Mixing characteristics both inside and outside the estuary determine the concentrations in this volume.

Non-tidal volume is primarily from two sources. First is river runoff. This is usually the major source. The second is "net non-tidal circulation." The latter is due to the circulation pattern within

the salt wedge (see Figure 8). As shown, more salt water can move into and out of the estuary than the tidal prism alone.

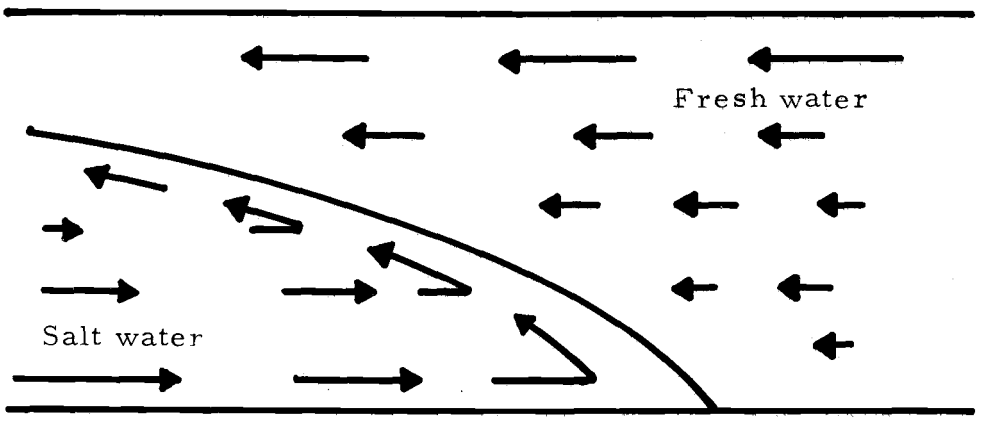

Figure 8. Non-tidal circulation.

The input into the estuary from the river is composed of water having a concentration C of material and a net runoff of R vol/unit time. It is then expected that the amount of matter transported by the river be C· R volume of matter/unit time. Similarly the volume transport multiplied by the concentration at the estuary-ocean interface determines the output of the estuary into the ocean. Since the volume transport in this case comes from different sources, and the concentrations in each source may be different, the analysis is more complicated. For example, when the tidal prism is stagnant, the water flowing out of the estuary is not renewed but merely returns on the next tide; the net transport due to tidal motion is zero. On the other

extreme, when the tidal prism is entirely renewed with each tide, the returning water has a zero concentration of the matter in question. The amount of matter transported out of the estuary by tidal motion during a tidal period is the concentration of matter in the tidal prism times one half the volume of the tidal prism. The same considerations must be given to computing the matter transported by the "net non-tidal" circulation. The concentrations in each of these portions of the flow are determined in a large part by the mixing characteristics involved. Establishing whether the matter influx is less than, equal to, or greater than the matter outflux will indicate whether the concentration within the estuary is decreasing, constant, or increasing.

III. INSTRUMENTATION

There were several instruments used in course of this experiment. The three component drag probe was used as a sensor for turbulent velocities. The signals from the drag probe as well as power to the drag probe were transmitted via a ten-conductor underwater cable. Drag probe signals were passed through a signal conditioning amplifier and then recorded on a Mid Western Instruments multichannel recording oscillograph. Water samples were collected in four National Institute of Oceanography (N. I. O.) sample bottles. Water thus collected was transferred into 250 ml. plastic bottles and standard glass salinity bottles for transport back to Corvallis. Analysis of these samples for particle size distribution and salinity was done in Corvallis. Salinity measurements were done using a Bisset-Berman salinometer. Particle Size analysis was performed using a Coulter Counter and a ND-2400 Pulse Height Analyzer.

The Salinometer, Oscillograph, N. I. O. Bottles, Coulter Counter and ND-2400 Pulse Height Analyzer are standard research instruments and standard procedures were followed in their use. Additional information about these instruments can be obtained from the operation manuals or from the manufacturers. The drag probe, power supply and a signal conditioning amplifier were built at Oregon State University. The power supply delivers plus or minus 15 volts direct current

at approximately 750 milliamperes. It is standard design which uses integrated circuits to provide voltage regulation. The signal conditioning amplifiers are designed to amplify an incoming signal by a factor of 1, 5, 10, 50, or 100 selectable by the operator. An adjustable offset level is also provided.

Since the drag probe is a rather unique instrument a brief description of its design and operation is included here. For a more detailed description of probe prior to modifications the reader is referred to Earle, 1971, or Earle, Groelle and Beardsley, 1970.

The Drag Probe

The drag probe consists of an inner sphere which is connected to the electronic case by a tapered rigid rod. An outer spherical shell surrounds the inner sphere and is supported by stainless steel springs. A drawing of the original drag probe appears in Figure 9. The inner sphere is rigidly fixed to the remainder of the instrument. The outer shell can move subject to the restraints imposed by the stainless steel springs. In operation, moving water exerts a force on the outer sphere. This force, opposed by the restoring force of the springs, results in a displacement of the outer sphere with respect to the inner sphere. Ferrite disks mounted on the outer shell opposite coils mounted inside the inner sphere act as variable inductors which measure the displacement electronically. The force exerted on the

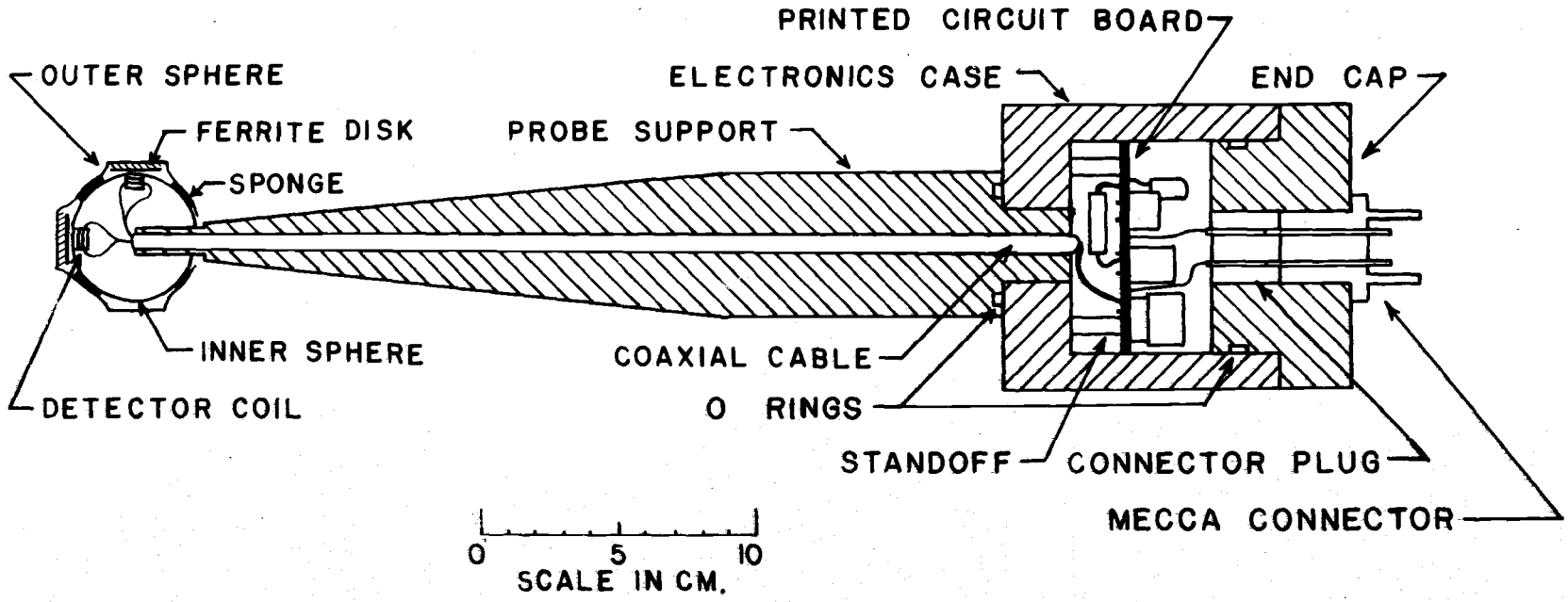

Figure 9. Three component drag probe.

outer sphere is related to the displacement through the spring constant. Since there are three sets of coils and discs, one set on each of three mutually perpendicular axes, the displacement, and the force can be resolved into its three spatial components. As indicated by Earle (1971) the components of force are related to the velocity components by the following equation:

$$F_i = \frac{1}{2} \rho A_i C_d u_i \; u \quad + C_m V \frac{du_i}{dt} \tag{3}$$

where F_i is the component of force in the i^{th} direction

ρ is the density of water

A_i is the projected cross sectional area in the i^{th} direction

C_d is the drag coefficient

C_m is the inertial coefficient

V is the volume of the sphere

The technique for determining the velocity components from the force components is discussed in the section on data handling.

Calibration

The following procedure was used to calibrate the drag probes. First the static force response was determined. This was accomplished by applying a known force along each axis and measuring the response. The calibration curves thus obtained can be found in

Appendix 1. The probe was then immersed in water and moved at a constant velocity along each axis in turn. The constant motion exerted a constant force. Thus the acceleration term in equation (3) is zero. When these results were compared to the static force test results the form of the drag coefficient was determined.

The frequency response was determined by immersing the drag probe in water and tapping each axis with a plastic rod. Each tap provided an impulse force and the response of the probe was recorded on the oscillograph. When considered as a one-degree of freedom damped harmonic oscillator it was found that the frequency for which the response was 3db down was 20 Hz.

Modifications

The original drag probe as described by Earle used sponge rubber to provide the restoring force between the spheres. Several factors indicated a change from sponge rubber was warranted. First it had a tendency to deteriorate after repeated exposure to salt water. Hysteresis, the failure to return to the original position after all forces were removed, complicated calibration. Finally, the markedly different response of wet sponge rubber and dry sponge rubber and the tendency for it to support plankton growth caused its rejection in favor of stainless steel coil springs. Stainless steel is virtually unaffected by salt water. It does not deteriorate to any appreciable extent which

means that the calibration data do not have to be continually updated. The hysteresis problem totally disappeared after the stainless steel springs were installed. The shape of the outer shell was changed from "almost spherical" to spherical. The protrusions used to seat the ferrite discs were eliminated. This resulted in closer agreement of the measured drag coefficient with the published results for drag coefficients of spheres from other sources. The shell was not split into hemispheres and reglued around the inner sphere, rather a smaller segment was cut out. This allowed all three ferrite discs to be mounted in the same section. Because the mutual perpendicularity of the discs was more readily achieved in this manner, crosstalk between axes was virtually eliminated.

Although the basic circuitry in the electronics package remained the same, the arrangement of the components was altered. By separating the circuit board into four sections, an oscillator and three detector-amplifier sections, crosstalk and interference in the electronics package was minimized. The substitution of a torroid coil for the standard inductor in the oscillator circuit eliminated the problem of signal drift and instability which was often encountered. Finally the components were arranged to facilitate trouble shooting and repair in the event of instrument failure. A schematic diagram of the electronic circuit is in Appendix 1.

IV. THE EXPERIMENT

An experiment was conducted on March 23 and 24, 1973, to measure turbulent velocities in the Yaquina Bay estuary and to examine the effects on mixing and suspension of particulate matter. The site of the experiment is shown in Figure 10. At noon Pacific Standard Time on the 23rd, divers working from the R. V. Paiute placed the sensor platform on the bottom of the estuary at the location marked X in the figure. When the platform was in position, two three-component drag probes were mounted on the extending arms. The platform was aligned so that the arms extended into the channel and were normal to the axis of the channel. The drag probes were mounted in such a way that one axis (axis 2) was vertical, another (axis 1) was parallel to the axis of the channel, and the third (axis 3) was normal to the first two, corresponding to the cross stream direction. One of the probes was mounted with the sensing head approximately 10 cm. above the bottom while the second was mounted with the sensor 100 cm. above the bottom. A ten conductor waterproof cable attached to the drag probes was then laid along the bottom to the Paiute dock (location A in Figure 10). There the cable was connected to the recording system.

Drag probe records were taken twice hourly for the first 12 hours of the experiment and twice every two hours for the last 12 hours. The records were taken approximately ten minutes before

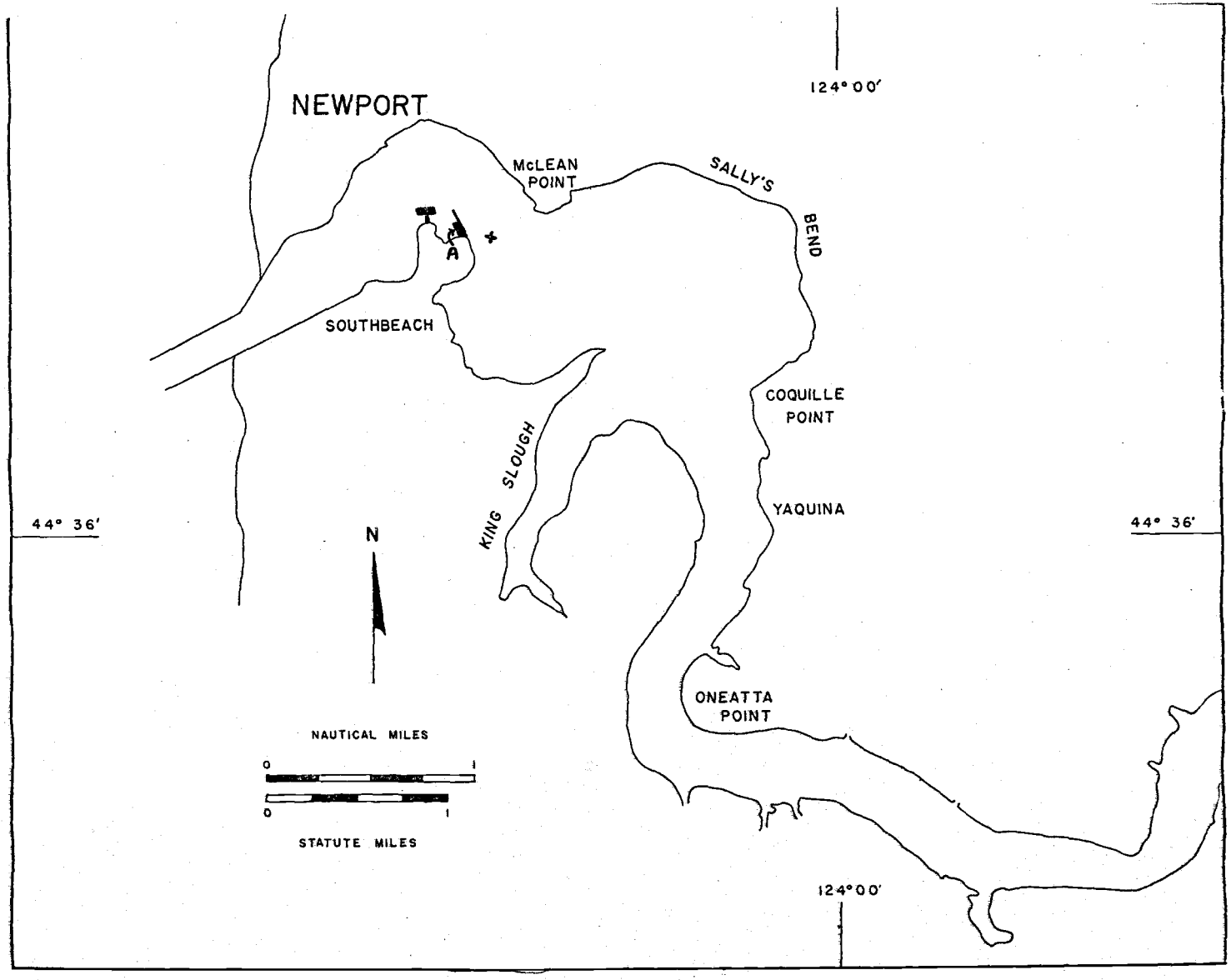

Figure 10. Yaquina Bay tidal estuary.

and ten minutes after the water samples were taken. Records were 30 seconds long. . When the records were first being taken, the signals from the probe at 10 cm did not exhibit the variability which was expected. Instead, the straight line trace which appeared lead to the assumption that this probe was not functioning properly. Therefore, the gain on the amplifiers which were receiving these signals was lowered so that the remaining traces from the 100 cm probe could be read more clearly. The velocity records which were analyzed in this project all came from the probe mounted 100 cm above the bottom. When the experiment was completed and the probes were examined in the laboratory, both probes functioned properly. It was not clear whether the probe at 10 cm failed to function or whether there was insufficient motion at that level to register on the probe.

Water samples were collected hourly on the half hour for the first 12 hours of the experiment and on the even half hours (2:30, 4:30, etc.) for the second 12 hours. The sampling bottles were attached to the hydrographic cable of the R. V. Paiute at 0. 5, 2. 5, 4. 5, and 6. 5 meters above the hydro weight. The hydro weight and its associated hardware accounted for another 50 cm so when the weight was on the bottom, the bottles were at 1, 3, 5, and 7 meters above the bottom. The cast was lowered until the weight just touched bottom. The bottles were then tripped by messenger and the samples were retrieved. The water from the samples which was to be

analyzed for salinity was transferred to standard salinity bottles for transport back to Corvallis and analysis there. The water which was to be analyzed for particulate matter was transferred into 250 ml. plastic bottles which had been rinsed with sulfuric acid to remove particulate matter and then distilled water to remove the acid. This is standard procedure for particulate matter analysis. These samples were also transported to Corvallis for analysis. Water samples were examined for particulate matter using a Coulter Counter and a ND-2400 Pulse Height analyzer and for salinity using a Bisset-Berman salinometer.

A surface float was attached to the drag probe platform by a heavy line. This, in addition to the many navigation buoys in the area, facilitated the return to the same location for each sampling. It also aided in the recovery of the instrumentation after the completion of the experiment.

V. HANDLING OF SAMPLES AND DATA PROCESSING

Water Samples

Water samples were collected in four National Institute of Oceanography (N. I. O.) sample bottles. To insure against contamination which may have occurred during a prior use or while in storage, the bottles used were washed in an acid bath and rinsed with distilled water prior to use. It is felt that the flushing which occurs during the hydro cast is sufficient to rinse out a bottle from a previous cast, provided the bottle was not originally contaminated. Samples for particle size analysis were drawn into 250 ml plastic bottles which were also washed in an acid bath and rinsed with distilled water prior to use. Salinity samples were drawn into standard glass salinity bottles according to normal procedure. Since analysis was done in Corvallis rather than at the sampling site the plastic bottles were stored in a light tight metal container to inhibit biological activity prior to their arrival in Corvallis. Between the time they arrived until the time the actual analysis took place the samples were under refrigeration to inhibit biological activity as well as chemical activity. Salinity bottles, once sealed, require no such special handling. Salinity determinations were obtained using a Bisset-Berman salinometer. The values of salinity measured appear in Table 1 and are plotted against depth in Figure 11.

Table 1. Salinity o/oo.

Cast #	1	2	4	5	6	7	8	9	10	
1	31.58	31.63	31.49	31.45	31.11	30.51	30.39	30.79	29.46	
3	31.05	31.68	31.46	31.12	31.11	30.29	29.70	25.29	29.49	
5	27.70	31.59	31.33	30.63	30.61	27.97	26.45	23.48	22.43	
7	17.16	24.28	29.75	29.50	26.99	24.04	22.01	19.61	20.57	
m. above			difference between top and bottom salinity o/oo							
bottom	14.42	7.35	1.74	1.95	4.12	6.47	8.38	11.18	8.89	

	11	12	13	14	15	16	17	18	
1	30.81	31.78	31.88	31.74	30.50	28.75	28.69	28.43	
3	30.52	31.80	31.95	31.85	30.44	28.37	26.64	28.39	
5	27.41	31.04	31.91	31.71	29.96	23.31	19.69	28.15	
7	21.48	24.55	31.56	31.63	24.44	17.82	16.73	17.85	ave. difference
m. above			difference between top and bottom salinity						
bottom	9.33	7.23	.32	.11	6.06	10.93	11.96	10.58	7.12

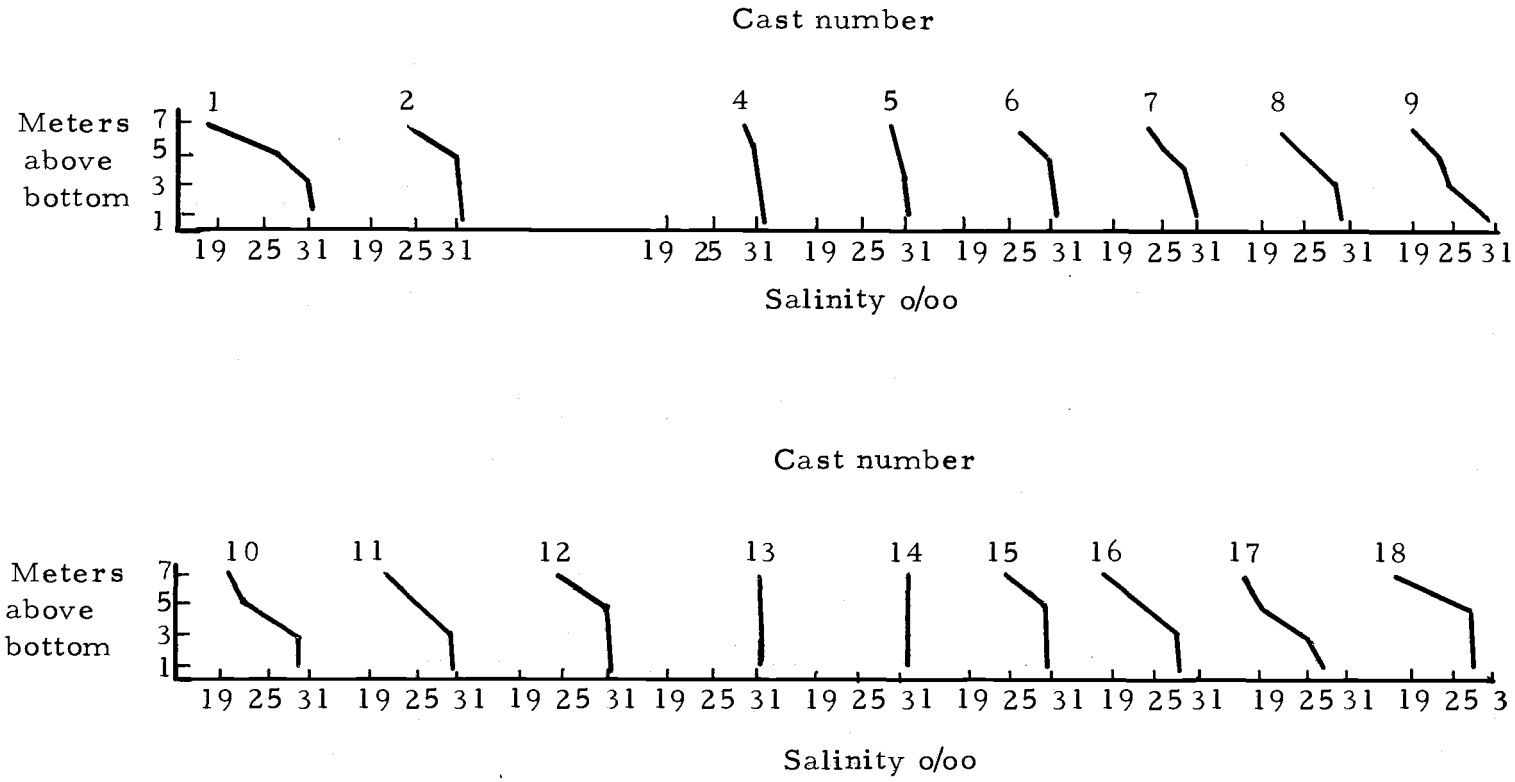

Figure 11. Salinity profiles.

Drag Probe Records

Drag probe records were taken at a chart speed of two inches per second. Each record was 30 seconds or 60 inches long. The records were digitized at the Oregon State University Computer Center using a manually operated digitizing machine. Since the cost of digitizing the entirety of each record by this method would have been prohibitive, a "representative" 24-inch section was taken from each of the records which corresponded to a run before the water samples were taken. The records taken before the water samples and those taken after were very similar in each case. The records thus selected were digitized at the rate of 100 samples per inch. This is equivalent to a sampling frequency of 200 Hz. This sampling rate is much more than sufficient to resolve to 10 Hz. The high sampling rate was used, however, to insure the convergence of the numerical method which was employed to resolve the velocity components from the components of force recorded by the drag probe. As indicated in the section on instrumentation (p. 18) the force which the water exerts on the outer sphere of the drag probe is related to the water velocity by equation (3), which is restated here.

$$F_i = \frac{1}{2} \rho A_i C_d u_i |u| + C_m V \frac{du_i}{dt} \qquad (4)$$

This equation was not solved analytically for the u_i as a function of the

F_i but rather the equation was rewritten as

$$u_i' = a\, u_i |u| + BF_i \tag{5}$$

where the prime denotes total derivative and a and B are collected coefficients from equation (3).

It can be shown that this system of equations is a stable system of ordinary differential equations whenever the values of $|u|$ are finite. The details of this are found in Appendix 2. Since the system is stable it lends itself to solution by various numerical methods for ordinary differential equations. The high sampling rate used in digitizing the data corresponds to a small step size in the numerical method. In general, the smaller the step size, the faster a numerical method will converge (Gear, 1971).

The numerical method chosen was a multistep method which used a third order Adams-Bashford predictor and a fourth order Adams-Moulton corrector. The Predictor-Corrector scheme is initiated with values derived by a fourth order Runge-Kutta method. The velocity records thus obtained were used to calculate various quantities. The Reynolds Stress Tensor $\tau_{ij} = \rho\, u_i u_j$ was calculated directly by averaging the values of $u_i(t)u_j(t)$ over the length of the record. The equation used was $\tau_{ij} = \frac{\rho}{N} \sum_{t=1}^{N} u_i(t)u_j(t)$ (6)

where: N = number of data points

t = time of the record

was computed for records 1, 2, 5 through 18. Record 3 was lost during processing and record 4 showed a zero velocity. Table 2 shows the six independent components of τ_{ij} for each of the records taken. The relative magnitudes the Reynolds Stress was estimated by using a norm of the sensor, τ_{ij} . The norm of matrix A can be defined as $\|A\| = \max \Sigma |A_i^j|$. The norm of a vector $\vec{a}$ consistent with the above matrix norm is defined as $\|\vec{a}\| = \sum_i a_i$. The relative vertical component of the Reynolds Stress can be illustrated by the norm of the product $e_3 \cdot \tau_{ij}$, where e_3 is the unit vector in the x_3 direction. The norms thus described are shown in Table 2.

The power spectra for each record was computed using a Fast Fourier Transform method (RSTFFT) available on the OS-3 system in the ARAND Time Series Analysis Package. The routine gives the Fourier Coefficients of the corresponding series of sines and cosines. These coefficients were band averaged to obtain the spectral estimates. The three dimensional energy spectra for each of the runs processed can be found in Table 3. They were obtained by adding the three components of energy at each frequency for which a spectral estimate was made. Plots of those spectra versus a non-dimensionalized wavenumber are found in Figures A through P in Appendix 3.

Table 2.

Run No.	Stress Tensor			Norm τ_{ij}	Norm τ_{i2}	Norm τ_{i3}
1	5.71 E 3	-1.68E 3	1.25E 3	9.09E3	3.44E3	2.13E3
		1.33E 3	-4.27E 2			
			4.57E 2			
2	1.91E 1	-3.60E-1	-1.29E 0	2.02E1	5.92E0	2.71E0
		4.96E 0	-6.06E-1			
			8.17E-1			
5	1.33E 3	1.28E 3	4.65E 2	3.16E3	3.08E3	1.10E3
		1.35E 3	4.46E 2			
			1.85E 2			
6	3.18E 3	-7.69E 2	-4.70E 2	4.65E3	1.19E3	7.09E2
		2.84E 2	1.36E 2			
			1.03E 2			
7	4.31E 3	1.44E 3	1.44E 3	7.24E3	2.74E3	2.93E3
		7.32E 2	5.64E 2			
			9.22E 2			
8	6.95E 4	-7.70E 4	5.14E 3	1.83E5	1.71E5	1.17E4
		8.83E 4	-6.01E 3			
			5.50E 2			
9	4.06E 4	-1.85E 3	-3.56E 3	4.74E4	3.46E3	4.25E3
		1.34E 3	2.69E 2			
			4.20E 2			

Table 2. (Continued)

Run No.	Stress Tensor			Norm τ_{ij}	Norm τ_{i2}	Norm τ_{i3}
10	2.64E 3	-2.12E 2	6.47E 1	9.36E3	2.57E2	7.95E1
		3.57E 1	-8.69E 0			
			6.13E 0			
11	1.01E 3	1.05E 3	-3.15E 2	2.51E3	2.59E3	7.93E2
		1.19E 3	-3.50E 2			
			1.28E 2			
12	5.49E 2	-2.20E 1	-9.91E 1	7.39E2	5.51E1	1.06E2
		2.44E 1	5.12E 0			
			2.11E 1			
13	1.15E 3	1.73E 4	7.81E 3	1.35E5	2.65E4	8.46E3
		8.46E 3	7.49E 2			
			7.03E 2			
14	7.36E 3	-1.12E 4	8.04E 2	3.79E4	3.79E4	2.59E3
		2.51E 4	-1.61E 3			
			1.73E 2			
15	3.38E 4	1.09E 4	1.78E 3	4.10E4	1.54E4	2.43E3
		4.03E 3	5.22E 2			
			1.23E 2			

Table 2. (Continued)

Run No.	Stress Tensor			Norm τ_{ij}	Norm τ_{i2}	Norm τ_{i3}
16	2.69E 4	-5.76E 3	-1.26E 3	3.06E4	7.91E3	1.67E3
		1.82E 3	3.26E 2			
			7.84E 1			
17	8.34E 4	3.29E 3	5.00E 3	9.07E4	1.16E4	6.38E3
		7.56E 3	-7.93E 2			
			5.84E 2			
18	2.50E 3	1.73E 2	-8.37E 2	3.51E3	3.02E2	1.20E3
		6.80E 1	-6.13E 1			
			3.02E 2			

Key: τ_{11} τ_{12} τ_{13}
τ_{22} τ_{23}
τ_{33}

Note: $\tau_{ij} = \tau_{ji}$

VI. DISCUSSION

In the absence of an instrument which could measure the three components of turbulent velocity, measurements of quantities such as the Reynolds stress tensor, τ_{ij}, and the three dimensional energy spectrum, E(k) dk, were impossible. All information about these quantities in sea water was either theoretical or inferred from measurements in the atmosphere by similarity theory. The capability of the drag probe to measure the three components of velocity, u, v, and w, now makes it possible to shed some light on these quantities from an experimental viewpoint. The three dimensional energy spectra were calculated for each run except numbers three and four. These spectral estimates were plotted against a non-dimensionalized wavenumber. The characteristic length used to non-dimensionalize the wavenumber was 100 cm, the distance the probe was above the bottom boundary. Figure 12 shows the three components of force as recorded directly by the oscillograph. Figure 13 shows the three components of velocity which were derived from the force records. Figure 14 shows the plot of the three dimensional energy spectrum against wavenumber. Each is for the eighth run. The plots of the energy spectra for the remaining runs can be found in Appendix 3.

Due to the intractibility of the complete equations of motion when applied to turbulent fluid flow, the problem of describing these

Figure 12. Force records.

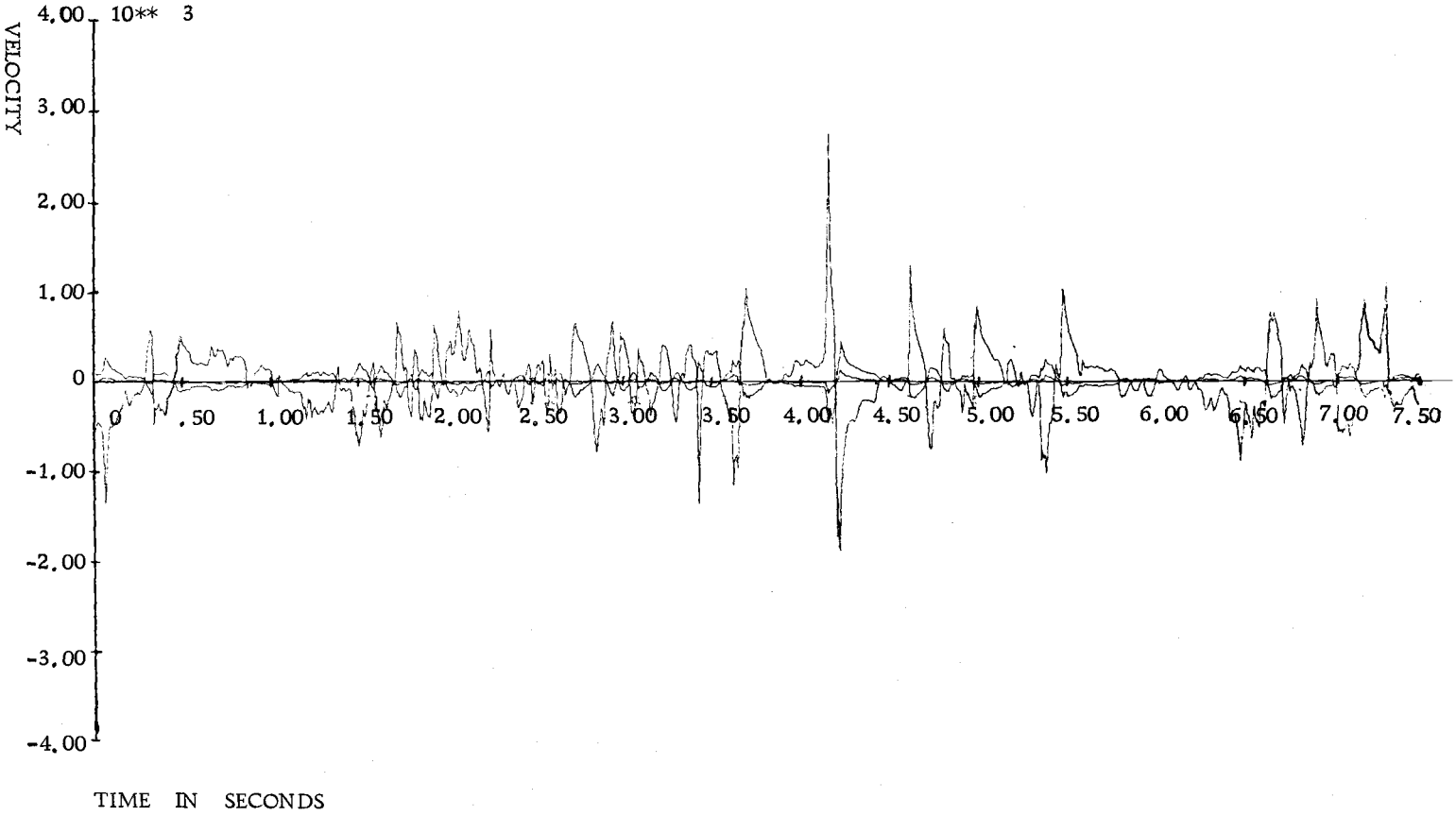

Figure 13. Velocity record.

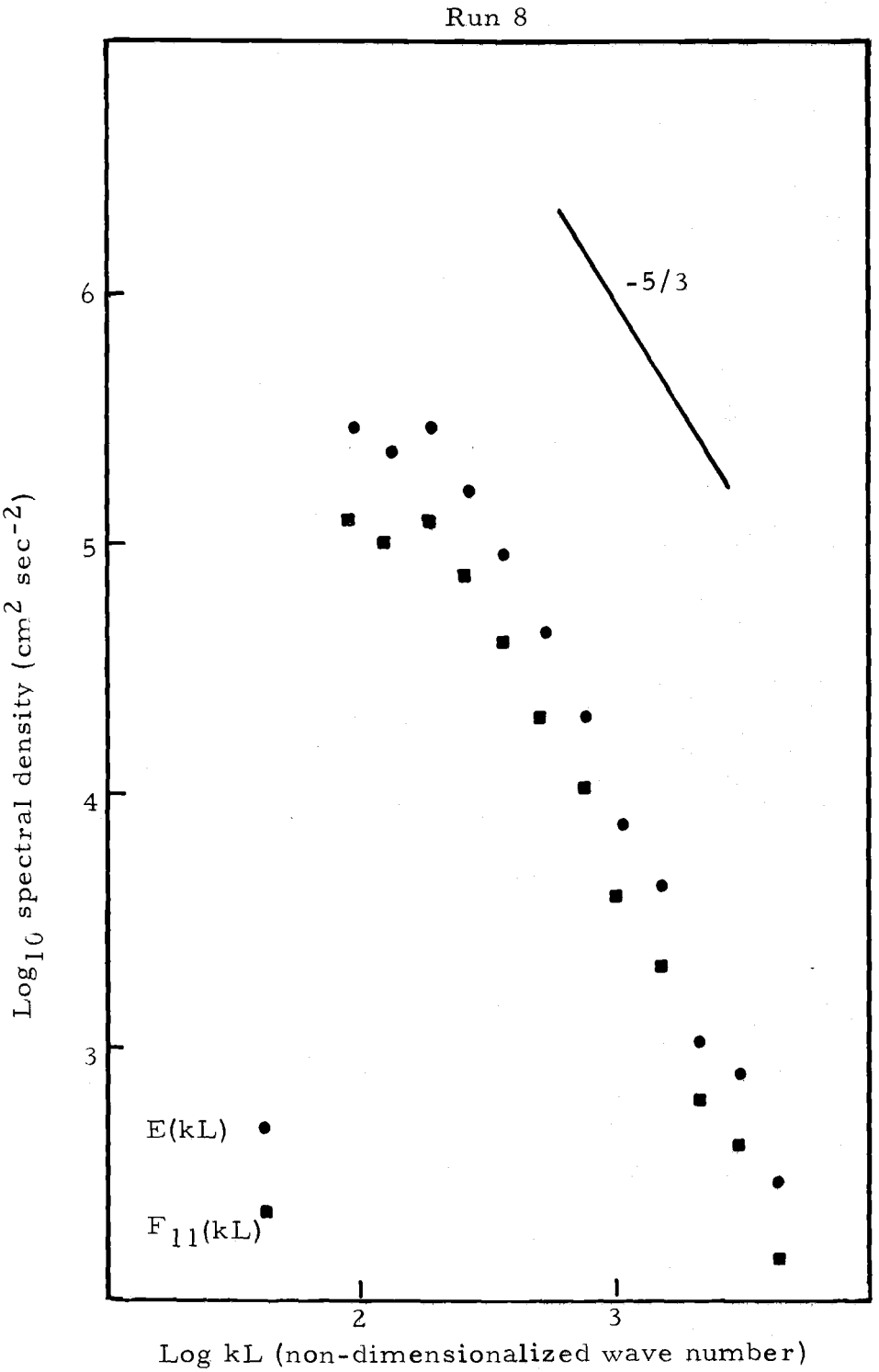

Figure 14. Energy spectra.

flows has been attacked by dividing the flow statistics into wavenumber ranges. The rationale behind this method is to determine under which conditions certain terms dominate the description of the flow to such an extent that the others can be ignored. After "solving" these simplified problems attempts are made to form a continuous solution by fitting together the ranges for which simplified solutions have been found. Tennekes and Lumley (1972) describe one such section called the inertial subrange. The condition necessary for the existence of the inertial subrange is that the eddy sizes in this range of wavenumbers not be directly affected by the mechanisms which produce or dissipate energy.

Let the criterion for a range of eddy sizes to be independent of the turbulent production processes be:

$$s(k)/S > 10$$

where $s(k) = (k^3 E(k))^{1/2}/2\pi$ is the characteristic rate of strain at the wavenumber k.

$S = S_{ij} = 1/2(\partial U_i/\partial x_j + \partial U_j/\partial x_i)$ is the mean rate of strain

E(k) is the turbulent kinetic energy at wavenumber k. Also, let the criterion for independence from the dissipative mechanism be given by:

$$S(k)/k^2 > 10$$

where is viscosity. Then for the flow to have an inertial subrange, the Reynolds number must be greater than 10^5. If the Reynolds numbers for the different runs are examined (Table 3) evidence of the inertial subrange in all but number 4 and possibly 2 can be expected. The range of wavenumbers which form the inertial subrange can be estimated by graphically interpreting (Figure 15). Table 3 shows the range of wavenumbers expected to be within the inertial subrange on the basis of graphical interpretation. It also shows the range of wavenumbers for which E(k) was calculated. Where these ranges overlapped, the curves of E(k) were examined for evidence of the -5/3 power relationship. Within the predicted inertial subrange, there is good agreement with the -5/3 power law in both the three dimensional energy spectra E(k), and the one dimensional energy spectra in the downstream direction $F_{11}(k)$ (Figures A-P, Appendix 3). At wavenumbers lower than those predicted for the inertial subrange, the tendency for the -5/3 slope remains. This indicates that the local rate of strain need not be an entire order of magnitude greater than the mean rate of strain for the spectra in that region to exhibit properties of the inertial subrange.

At smaller wavenumbers the geometry of the particular flow is thought to be important. If viscosity effects are ignored at these smaller wavenumbers, the relevant parameters determining the

Table 3. Spectral analysis of velocity records.

RUN NUMBER:1
MEAN VELOCITY:20.7 CM/SEC TURBULENT VELOCITY SCALE:50 CM/SEC
REYNOLDS NUMBER= 0.454546E+07 INERTIAL SUBRANGE 3.5E2 < KL <:5.2E3

SPECT.EST.	HZ	KL	F(KL)	L(KL)	L(KE/VV)
:.169400E 5 =	0.1025=	0.311124E+01=	0.395342E+00=	0.4929=-0.6761
:.403600E 4 =	0.1425=	0.432538E+01=	0.941912E-01=	0.6360=-1.1560
:.517500E 4 =	0.2025=	0.614659E+01=	0.120773E+00=	0.7886=-0.8954
:.389500E 4 =	0.2825=	0.857487E+01=	0.909006E-01=	0.9332=-0.8742
:.263600E 4 =	0.4025=	0.122173E+02=	0.615183E-01=	1.0870=-0.8900
:.117560E 4 =	0.5625=	0.170739E+02=	0.274359E-01=	1.2323=-1.0954
:.903500E 3 =	0.8025=	0.243587E+02=	0.210857E-01=	1.3867=-1.0554
:.650900E 3 =	1.1225=	0.340718E+02=	0.151906E-01=	1.5324=-1.0520
:.650000E 3 =	1.6025=	0.486415E+02=	0.151696E-01=	1.6870=-0.8980
:.430460E 3 =	2.2425=	0.680678E+02=	0.100460E-01=	1.8329=-0.9311
:.219670E 3 =	3.2025=	0.972072E+02=	0.512661E-02=	1.9877=-1.0685
:.107350E 3 =	4.4825=	0.136060E+03=	0.250531E-02=	2.1337=-1.2334

RUN NUMBER:2
MEAN VELOCITY:10.9 CM/SEC TURBULENT VELOCITY SCALE:3 CM/SEC
REYNOLDS NUMBER= 0.272727E+06 INERTIAL SUBRANGE 3.5E2 < KL <:7.0E2

SPECT.EST.	HZ	KL	F(KL)	L(KL)	L(KE/VV)
:.267200E 2 =	0.1025=	0.590849E+01=	0.224897E-02=	0.7715=-0.7559
:.126540E 2 =	0.1425=	0.821425E+01=	0.106506E-02=	0.9146=-0.9375
:.837900E 1 =	0.2025=	0.116729E+02=	0.705244E-03=	1.0672=-0.9639
:.439200E 1 =	0.2825=	0.162844E+02=	0.369666E-03=	1.2118=-1.0998
:.430200E 1 =	0.4025=	0.232017E+02=	0.362091E-03=	1.3655=-0.9551
:.257800E 1 =	0.5625=	0.324247E+02=	0.216985E-03=	1.5109=-1.0321
:.123680E 1 =	0.8025=	0.462592E+02=	0.104099E-03=	1.6652=-1.1967
:.468000E 0 =	1.1225=	0.647052E+02=	0.393906E-04=	1.8109=-1.4731
:.210740E 0 =	1.6025=	0.923743E+02=	0.177376E-04=	1.9655=-1.6649
:.114570E 0 =	2.2425=	0.129266E+03=	0.964313E-05=	2.1115=-1.7837
:.107910E 0 =	3.2025=	0.184605E+03=	0.908257E-05=	2.2662=-1.6549
:.757100E-1 =	4.4825=	0.258389E+03=	0.637236E-05=	2.4123=-1.6628

RUN NUMBER:5
MEAN VELOCITY:2.93 CM/SEC TURBULENT VELOCITY SCALE:31 CM/SEC
REYNOLDS NUMBER= 0.281818E+07 INERTIAL SUBRANGE 3.5E2 < KL <:3.9E3

SPECT.EST.	HZ	KL	F(KL)	L(KL)	L(KE/VV)
:.229900E 4 =	0.1025=	0.219804E+02=	0.267796E+01=	1.3420=-0.2792
:.930700E 3 =	0.1425=	0.305581E+02=	0.108411E+01=	1.4851=-0.5288
:.593300E 3 =	0.2025=	0.434247E+02=	0.691097E+00=	1.6377=-0.5717
:.169700E 3 =	0.2825=	0.605801E+02=	0.197673E+00=	1.7823=-0.9707
:.116200E 3 =	0.4025=	0.863133E+02=	0.135354E+00=	1.9361=-0.9814
:.633900E 2 =	0.5625=	0.120624E+03=	0.738390E-01=	2.0814=-1.0993
:.199200E 2 =	0.8025=	0.172091E+03=	0.232035E-01=	2.2358=-1.4477
:.616000E 1 =	1.1225=	0.240712E+03=	0.717539E-02=	2.3815=-1.8116
:.262900E 1 =	1.6025=	0.343645E+03=	0.306235E-02=	2.5361=-2.0268
:.112500E 1 =	2.2425=	0.480889E+03=	0.131044E-02=	2.6820=-2.2495
:.783000E 0 =	3.2025=	0.686754E+03=	0.912067E-03=	2.8368=-2.2522
:.488000E 0 =	4.4825=	0.961241E+03=	0.568440E-03=	2.9828=-2.3115

Table 3. (Continued)

RUN NUMBER:6
MEAN VELOCITY:7.4 CM/SEC TURBULENT VELOCITY SCALE:34 CM/SEC
REYNOLDS NUMBER= 0.309091E+07 INERTIAL SUBRANGE 3.5E2 < KL <:4.1E3

SPECT.EST.	HZ	KL	F(KL)	L(KL)	L(KE/VV)
:.464500E 4 =	0.1025=	0.870305E+01=	0.848247E+00=	0.9397=-0.4568	
:.359400E 4 =	0.1425=	0.120994E+02=	0.656319E+00=	1.0828=-0.4246	
:.295900E 4 =	0.2025=	0.171938E+02=	0.540358E+00=	1.2354=-0.3564	
:.289640E 4 =	0.2825=	0.239865E+02=	0.528926E+00=	1.3800=-0.2211	
:.121040E 4 =	0.4025=	0.341754E+02=	0.221037E+00=	1.5337=-0.4463	
:.562600E 3 =	0.5625=	0.477607E+02=	0.102739E+00=	1.6791=-0.6337	
:.208040E 3 =	0.8025=	0.681385E+02=	0.379912E-01=	1.8334=-0.9114	
:.361800E 2 =	1.1225=	0.953090E+02=	0.660701E-02=	1.9791=-1.5254	
:.162500E 2 =	1.6025=	0.136065E+03=	0.296749E-02=	2.1337=-1.7184	
:.798600E 1 =	2.2425=	0.190406E+03=	0.145836E-02=	2.2797=-1.8809	
:.294300E 1 =	3.2025=	0.271917E+03=	0.537436E-03=	2.4344=-2.1597	
:.149800E 1 =	4.4825=	0.380599E+03=	0.273557E-03=	2.5805=-2.3070	

RUN NUMBER:7
MEAN VELOCITY:21.8 CM/SEC TURBULENT VELOCITY SCALE:45 CM/SEC
REYNOLDS NUMBER= 0.409091E+07 INERTIAL SUBRANGE 3.5E2 < KL <:5.2E3

SPECT.EST.	HZ	KL	F(KL)	L(KL)	L(KE/VV)
:.183700E 5 =	0.1025=	0.295425E+01=	0.386542E+00=	0.4705=-0.5719	
:.866000E 4 =	0.1425=	0.410713E+01=	0.182224E+00=	0.6135=-0.7554	
:.632000E 4 =	0.2025=	0.583644E+01=	0.132986E+00=	0.7662=-0.7396	
:.493000E 4 =	0.2825=	0.814219E+01=	0.103737E+00=	0.9107=-0.7028	
:.155600E 4 =	0.4025=	0.116008E+02=	0.327414E-01=	1.0645=-1.0499	
:.131400E 4 =	0.5625=	0.162123E+02=	0.276492E-01=	1.2098=-0.9780	
:.587100E 3 =	0.8025=	0.231296E+02=	0.123538E-01=	1.3642=-1.1735	
:.171700E 3 =	1.1225=	0.323526E+02=	0.361291E-02=	1.5099=-1.5617	
:.668000E 2 =	1.6025=	0.461871E+02=	0.140561E-02=	1.6645=-1.8171	
:.352100E 2 =	2.2425=	0.646332E+02=	0.740889E-03=	1.8105=-1.9493	
:.136780E 2 =	3.2025=	0.923022E+02=	0.287813E-03=	1.9652=-2.2052	
:.679600E 1 =	4.4825=	0.129194E+03=	0.143002E-03=	2.1112=-2.3629	

RUN NUMBER:8
MEAN VELOCITY:0.66 CM/SEC TURBULENT VELOCITY SCALE:230 CM/SEC
REYNOLDS NUMBER= 0.209091E+08 INERTIAL SUBRANGE 3.5E2 < KL <:1.8E4

SPECT.EST.	HZ	KL	F(KL)	L(KL)	L(KE/VV)
:.296983E 6 =	0.1025=	0.975797E+02=	0.681779E+04=	1.9894= 0.7386	
:.235240E 6 =	0.1425=	0.135660E+03=	0.540037E+04=	2.1324= 0.7805	
:.297090E 6 =	0.2025=	0.192772E+03=	0.682025E+04=	2.2851= 1.0345	
:.170000E 6 =	0.2825=	0.268939E+03=	0.390264E+04=	2.4296= 0.9367	
:.916090E 5 =	0.4025=	0.383179E+03=	0.210305E+04=	2.5834= 0.8219	
:.439985E 5 =	0.5625=	0.535498E+03=	0.101007E+04=	2.7287= 0.6487	
:.209466E 5 =	0.8025=	0.763977E+03=	0.480868E+03=	2.8831= 0.4807	
:.744860E 4 =	1.1225=	0.106862E+04=	0.170996E+03=	3.0288= 0.1774	
:.407494E 4 =	1.6025=	0.152558E+04=	0.935477E+02=	3.1834= 0.0701	
:.192553E 4 =	2.2425=	0.213485E+04=	0.235429E+02=	3.3294=-0.3831	
:.758290E 3 =	3.2025=	0.304877E+04=	0.174079E+02=	3.4841=-0.3595	
:.287623E 3 =	4.4825=	0.426733E+04=	0.660291E+01=	3.6301=-0.6345	

Table 3. (Continued)

RUN NUMBER:9
MEAN VELOCITY:34.5 CM/SEC TURBULENT VELOCITY SCALE:118 CM/SEC
REYNOLDS NUMBER= 0.107273E+08 INERTIAL SUBRANGE 3.5E2 < KL <:1.1E4

SPECT.EST.	HZ	KL	F(KL)	L(KL)	L(KE/VV)
:.614890E 5 =	0.1025=	0.186674E+01=	0.516606E+00=	0.2711=-	1.0839
:.115180E 6 =	0.1425=	0.259523E+01=	0.967696E+00=	0.4142=-	0.6682
:.396410E 5 =	0.2025=	0.368795E+01=	0.333048E+00=	0.5668=-	0.9788
:.281570E 5 =	0.2825=	0.514492E+01=	0.236564E+00=	0.7114=-	0.9828
:.131260E 5 =	0.4025=	0.733038E+01=	0.110279E+00=	0.8651=-	1.1605
:.621250E 4 =	0.5625=	0.102443E+02=	0.521949E-01=	1.0105=-	1.3400
:.431560E 4 =	0.8025=	0.146152E+02=	0.362579E-01=	1.1648=-	1.3439
:.150930E 4 =	1.1225=	0.204431E+02=	0.126805E-01=	1.3105=-	1.6544
:.266270E 3 =	1.6025=	0.291849E+02=	0.223709E-02=	1.4652=-	2.2533
:.163560E 3 =	2.2425=	0.408407E+02=	0.137417E-02=	1.6111=-	2.3190
:.762790E 2 =	3.2025=	0.583243E+02=	0.640865E-03=	1.7658=-	2.4955
:.320450E 2 =	4.4825=	0.816358E+02=	0.269229E-03=	1.9119=-	2.7261

RUN NUMBER:10
MEAN VELOCITY:13.2 CM/SEC TURBULENT VELOCITY SCALE:29 CM/SEC
REYNOLDS NUMBER= 0.263636E+07 INERTIAL SUBRANGE 3.5E2 < KL <:3.7E3

SPECT.EST.	HZ	KL	F(KL)	L(KL)	L(KE/VV)
:.370845E 4 =	0.1025=	0.487898E+01=	0.212836E+00=	0.6883=-	0.6673
:.149712E 4 =	0.1425=	0.678298E+01=	0.859229E-01=	0.8314=-	0.9181
:.147112E 4 =	0.2025=	0.963897E+01=	0.844307E-01=	0.9840=-	0.7731
:.102269E 4 =	0.2825=	0.134470E+02=	0.586943E-01=	1.1286=-	0.7864
:.367045E 3 =	0.4025=	0.191589E+02=	0.210655E-01=	1.2824=-	1.0777
:.216347E 3 =	0.5625=	0.267749E+02=	0.124166E-01=	1.4277=-	1.1619
:.862810E 2 =	0.8025=	0.381989E+02=	0.495185E-02=	1.5821=-	1.4068
:.215679E 2 =	1.1225=	0.534308E+02=	0.123783E-02=	1.7278=-	1.8632
:.598600E 1 =	1.6025=	0.762787E+02=	0.343549E-03=	1.8824=-	2.2653
:.440630E 1 =	2.2425=	0.106743E+03=	0.252887E-03=	2.0283=-	2.2524
:.290510E 1 =	3.2025=	0.152439E+03=	0.166730E-03=	2.1831=-	2.2785
:.228070E 1 =	4.4825=	0.213366E+03=	0.130894E-03=	2.3291=-	2.2376

RUN NUMBER:11
MEAN VELOCITY:10.3 CM/SEC TURBULENT VELOCITY SCALE:28 CM/SEC
REYNOLDS NUMBER= 0.254546E+07 INERTIAL SUBRANGE 3.5E2 < KL <:3.1E3

SPECT.EST.	HZ	KL	F(KL)	L(KL)	L(KE/VV)
:.392500E 4 =	0.1025=	0.625268E+01=	0.369969E+00=	0.7961=-	0.5044
:.101310E 4 =	0.1425=	0.869275E+01=	0.954944E-01=	0.9392=-	0.9495
:.141380E 4 =	0.2025=	0.123529E+02=	0.133264E+00=	1.0918=-	0.6522
:.462700E 3 =	0.2825=	0.172330E+02=	0.436139E-01=	1.2364=-	0.9927
:.998600E 2 =	0.4025=	0.245532E+02=	0.941277E-02=	1.3901=-	1.5048
:.900400E 2 =	0.5625=	0.343135E+02=	0.848714E-02=	1.5355=-	1.4044
:.376800E 2 =	0.8025=	0.489539E+02=	0.355170E-02=	1.6898=-	1.6284
:.156760E 2 =	1.1225=	0.684745E+02=	0.147761E-02=	1.8355=-	1.8635
:.880200E 1 =	1.6025=	0.977553E+02=	0.829673E-03=	1.9901=-	1.9596
:.732200E 1 =	2.2425=	0.136797E+03=	0.690169E-03=	2.1361=-	1.8936
:.612800E 1 =	3.2025=	0.195358E+03=	0.577623E-03=	2.2908=-	1.8162
:.410650E 1 =	4.4825=	0.273440E+03=	0.387077E-03=	2.4369=-	1.8440

Table 3. (Continued)

RUN NUMBER:12
MEAN VELOCITY:19 CM/SEC TURBULENT VELOCITY SCALE:14 CM/SEC
REYNOLDS NUMBER= 0.127273E+07 INERTIAL SUBRANGE 3.5E2 < KL <:2.1E3

SPECT.EST.	HZ	KL	F(KL)	L(KL)	L(KE/VV)
:.115650E 4 =	0.1025=	0.338961E+01=	0.320360E-01=	0.5302=	-0.6990
:.791100E 3 =	0.1425=	0.471239E+01=	0.219141E-01=	0.6732=	-0.7208
:.397000E 3 =	0.2025=	0.669655E+01=	0.109972E-01=	0.8259=	-0.8676
:.276170E 3 =	0.2825=	0.934210E+01=	0.765014E-02=	0.9704=	-0.8806
:.936000E 2 =	0.4025=	0.133104E+02=	0.259280E-02=	1.1242=	-1.1968
:.285240E 2 =	0.5625=	0.186015E+02=	0.790138E-03=	1.2695=	-1.5675
:.144930E 2 =	0.8025=	0.265382E+02=	0.401468E-03=	1.4239=	-1.7072
:.726400E 1 =	1.1225=	0.371204E+02=	0.201219E-03=	1.5696=	-1.8615
:.272520E 1 =	1.6025=	0.529937E+02=	0.754903E-04=	1.7242=	-2.1326
:.984200E 0 =	2.2425=	0.741581E+02=	0.272632E-04=	1.8702=	-2.4290
:.623000E 0 =	3.2025=	0.105905E+03=	0.172576E-04=	2.0249=	-2.4728
:.397500E 0 =	4.4825=	0.148234E+03=	0.110111E-04=	2.1709=	-2.5220

RUN NUMBER:13
MEAN VELOCITY:48.4 CM/SEC TURBULENT VELOCITY SCALE:204 CM/SEC
REYNOLDS NUMBER= 0.185455E+08 INERTIAL SUBRANGE 3.5E2 < KL <:1.6E4

SPECT.EST.	HZ	KL	F(KL)	L(KL)	L(KE/VV)
:.127581E 6 =	0.1025=	0.133063E+01=	0.544622E+00=	0.1241=	-1.3894
:.939700E 5 =	0.1425=	0.184990E+01=	0.401142E+00=	0.2672=	-1.3791
:.117644E 6 =	0.2025=	0.262881E+01=	0.502203E+00=	0.4198=	-1.1289
:.528500E 5 =	0.2825=	0.366735E+01=	0.225608E+00=	0.5644=	-1.3319
:.473770E 5 =	0.4025=	0.522517E+01=	0.202245E+00=	0.7181=	-1.2256
:.319510E 5 =	0.5625=	0.730225E+01=	0.136394E+00=	0.8635=	-1.2513
:.149077E 5 =	0.8025=	0.104179E+02=	0.636385E-01=	1.0178=	-1.4281
:.560900E 4 =	1.1225=	0.145721E+02=	0.239439E-01=	1.1635=	-1.7069
:.261190E 4 =	1.6025=	0.208033E+02=	0.111498E-01=	1.3181=	-1.8842
:.128234E 4 =	2.2425=	0.291116E+02=	0.547410E-02=	1.4641=	-2.0472
:.730980E 3 =	3.2025=	0.415742E+02=	0.312043E-02=	1.6188=	-2.1365
:.360240E 3 =	4.4825=	0.581908E+02=	0.153781E-02=	1.7649=	-2.2978

RUN NUMBER:14
MEAN VELOCITY:8.3 CM/SEC TURBULENT VELOCITY SCALE:104 CM/SEC
REYNOLDS NUMBER= 0.945455E+07 INERTIAL SUBRANGE 3.5E2 < KL <:9.6E3

SPECT.EST.	HZ	KL	F(KL)	L(KL)	L(KE/VV)
:.403190E 5 =	0.1025=	0.775935E+01=	0.585267E+01=	0.8898=	-0.5387
:.330570E 5 =	0.1425=	0.107874E+02=	0.479852E+01=	1.0329=	-0.4819
:.326960E 5 =	0.2025=	0.153295E+02=	0.474612E+01=	1.1855=	-0.3341
:.227940E 5 =	0.2825=	0.213855E+02=	0.330875E+01=	1.3301=	-0.3461
:.200967E 5 =	0.4025=	0.304697E+02=	0.291722E+01=	1.4839=	-0.2471
:.944570E 4 =	0.5625=	0.425818E+02=	0.137113E+01=	1.6292=	-0.4296
:.493140E 4 =	0.8025=	0.607500E+02=	0.715837E+00=	1.7835=	-0.5576
:.261510E 4 =	1.1225=	0.849743E+02=	0.379605E+00=	1.9293=	-0.6873
:.237509E 4 =	1.6025=	0.121311E+03=	0.344766E+00=	2.0839=	-0.5745
:.188855E 4 =	2.2425=	0.169760E+03=	0.274140E+00=	2.2298=	-0.5281
:.159365E 4 =	3.2025=	0.242432E+03=	0.231333E+00=	2.3846=	-0.4471
:.102545E 4 =	4.4825=	0.339330E+03=	0.148853E+00=	2.5306=	-0.4925

Table 3. (Continued)

RUN NUMBER:15
MEAN VELOCITY:4.1 CM/SEC TURBULENT VELOCITY SCALE:113 CM/SEC
REYNOLDS NUMBER= 0.102727E+08 INERTIAL SUBRANGE 3.5E2 < KL <:1.0E4

SPECT.EST.		HZ		KL		F(KL)		L(KL)	L(KE/VV)
:.756760E 5	=	0.1025=	0.157080E+02=	0.450185E+02=	1.1961=-0.0311
:.661600E 5	=	0.1425=	0.218379E+02=	0.393575E+02=	1.3392= 0.0537
:.310660E 5	=	0.2025=	0.310328E+02=	0.184807E+02=	1.4918=-0.1221
:.181416E 5	=	0.2825=	0.432926E+02=	0.107922E+02=	1.6364=-0.2111
:.205834E 5	=	0.4025=	0.616825E+02=	0.122447E+02=	1.7902=-0.0025
:.910010E 4	=	0.5625=	0.862022E+02=	0.541350E+01=	1.9355=-0.2116
:.191802E 4	=	0.8025=	0.122982E+03=	0.114100E+01=	2.0898=-0.7335
:.106621E 4	=	1.1225=	0.172021E+03=	0.634271E+00=	2.2356=-0.8427
:.424490E 3	=	1.6025=	0.245580E+03=	0.252522E+00=	2.3902=-1.0881
:.180743E 3	=	2.2425=	0.343659E+03=	0.107521E+00=	2.5361=-1.3130
:.111296E 3	=	3.2025=	0.490778E+03=	0.662082E-01=	2.6909=-1.3688
:.432384E 2	=	4.4825=	0.686936E+03=	0.257218E-01=	2.8369=-1.6334

RUN NUMBER:16
MEAN VELOCITY:20.9 CM/SEC TURBULENT VELOCITY SCALE:98 CM/SEC
REYNOLDS NUMBER= 0.890909E+07 INERTIAL SUBRANGE 3.5E2 < KL <:9.3E3

SPECT.EST.		HZ		KL		F(KL)		L(KL)	L(KE/VV)
:.517480E 5	=	0.1025=	0.308146E+01=	0.118468E+01=	0.4888=-0.7798
:.606200E 5	=	0.1425=	0.428399E+01=	0.138779E+01=	0.6319=-0.5680
:.323088E 5	=	0.2025=	0.608777E+01=	0.739653E+00=	0.7845=-0.6887
:.227351E 5	=	0.2825=	0.849281E+01=	0.520480E+00=	0.9291=-0.6967
:.144608E 5	=	0.4025=	0.121004E+02=	0.331055E+00=	1.0828=-0.7395
:.720140E 4	=	0.5625=	0.169105E+02=	0.164864E+00=	1.2282=-0.8969
:.246424E 4	=	0.8025=	0.241256E+02=	0.564144E-01=	1.3825=-1.2083
:.938840E 3	=	1.1225=	0.337458E+02=	0.214931E-01=	1.5282=-1.4816
:.509531E 3	=	1.6025=	0.481760E+02=	0.116648E-01=	1.6828=-1.5924
:.236100E 3	=	2.2425=	0.674164E+02=	0.540510E-02=	1.8288=-1.7806
:.105531E 3	=	3.2025=	0.962770E+02=	0.241595E-02=	1.9835=-1.9755
:.496232E 2	=	4.4825=	0.134758E+03=	0.113604E-02=	2.1295=-2.1572

RUN NUMBER:17
MEAN VELOCITY:7.1 CM/SEC TURBULENT VELOCITY SCALE:175 CM/SEC
REYNOLDS NUMBER= 0.159091E+08 INERTIAL SUBRANGE 3.5E2 < KL <:1.4E4

SPECT.EST.		HZ		KL		F(KL)		L(KL)	L(KE/VV)
:.163948E 6	=	0.1025=	0.907079E+01=	0.325229E+02=	0.9576=-0.3137
:.577270E 5	=	0.1425=	0.126106E+02=	0.104596E+02=	1.1007=-0.6633
:.512980E 5	=	0.2025=	0.179203E+02=	0.101762E+02=	1.2533=-0.5226
:.510030E 5	=	0.2825=	0.250000E+02=	0.101176E+02=	1.3979=-0.3805
:.337550E 5	=	0.4025=	0.356194E+02=	0.669609E+01=	1.5517=-0.4061
:.223700E 5	=	0.5625=	0.497787E+02=	0.443761E+01=	1.6970=-0.4394
:.151186E 5	=	0.8025=	0.710176E+02=	0.299913E+01=	1.8514=-0.4552
:.666800E 4	=	1.1225=	0.993362E+02=	0.132275E+01=	1.9971=-0.6650
:.321587E 4	=	1.6025=	0.141814E+03=	0.637943E+00=	2.1517=-0.8271
:.127870E 4	=	2.2425=	0.198451E+03=	0.253660E+00=	2.2976=-1.0817
:.768052E 3	=	3.2025=	0.283407E+03=	0.152361E+00=	2.4524=-1.1483
:.375780E 3	=	4.4825=	0.396681E+03=	0.745447E-01=	2.5984=-1.3127

Table 3. (Continued)

RUN NUMBER:18
MEAN VELOCITY:10.1 CM/SEC TURBULENT VELOCITY SCALE:31 CM/SEC
REYNOLDS NUMBER= 0.281818E+07 INERTIAL SUBRANGE 3.5E2 < KL <:3.9E3

SPECT.EST.	HZ	KL	F(KL)	L(KL)	L(KE/VV)
:.339630E 4 =	0.1025=	0.637649E+01=	0.332938E+00=	0.8046=	-0.6471
:.185980E 4 =	0.1425=	0.886488E+01=	0.182316E+00=	0.9477=	-0.7656
:.324860E 4 =	0.2025=	0.125975E+02=	0.318459E+00=	1.1003=	-0.3708
:.141580E 4 =	0.2825=	0.175742E+02=	0.138790E+00=	1.2449=	-0.5869
:.815400E 3 =	0.4025=	0.250394E+02=	0.799333E-01=	1.3986=	-0.6727
:.410000E 3 =	0.5625=	0.349930E+02=	0.401921E-01=	1.5440=	-0.8260
:.121900E 3 =	0.8025=	0.499233E+02=	0.119498E-01=	1.6983=	-1.1984
:.627600E 2 =	1.1225=	0.698304E+02=	0.615234E-02=	1.8440=	-1.3410
:.199400E 2 =	1.6025=	0.996910E+02=	0.195471E-02=	1.9987=	-1.6843
:.114800E 2 =	2.2425=	0.139505E+03=	0.112538E-02=	2.1446=	-1.7782
:.486600E 1 =	3.2025=	0.199227E+03=	0.477012E-03=	2.2993=	-1.9962
:.245500E 1 =	4.4825=	0.278855E+03=	0.240663E-03=	2.4454=	-2.1473

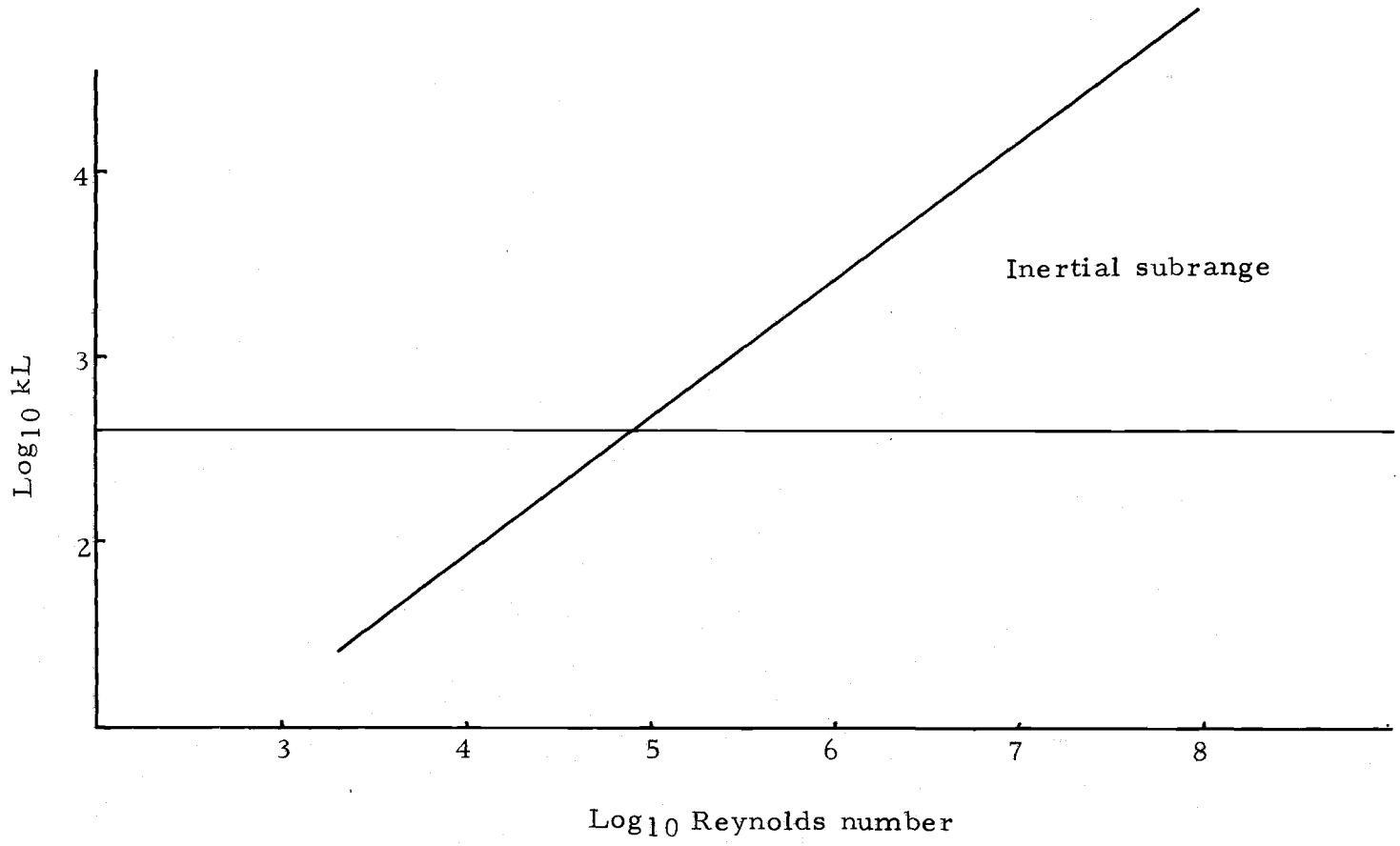
Inertial subrange
Log_{10} kL
4
3
2
3
4
5
6
7
8
Log_{10} Reynolds number

Figure 15.

energy spectra should be the mean strain rate, S, the dissipation or transfer, and the wavenumber K. Nondimensionalizing E(k) gives the function $E(k)/u^2l = F(kl)$. F(kl) should be similar in flows with similar geometries. Using the values previously found for E(k), u, and l, F(kl) was evaluated for each run. The results are plotted in Figure 16. Although there is considerable scatter in the data, the function F(kl) appears to be related to kl by a power law of approximately -5/3. The effect of the geometry changes since the river runoff and the tidal flow occupy different positions in the channel at different times in the tidal cycle. This was suspected due to the bends in the channel upstream and downstream of the experiment site and was confirmed by a series of salinity sections taken in the area during a previous experiment (Figures A, B and C, Appendix 4). Since the flow occupies different parts of the channel at different times, it experiences different geometries which could explain some of the scatter. In addition, the more obvious change from upstream flow to downstream flow exerts a significant influence. When the runs on an incoming tide are differentiated from those on an outgoing tide the scatter decreases. This is illustrated in Figure 17.

Figure 10 shows Yaquina Bay tidal estuary. Kulm and Byrne (1967) described it as having an area of approximately 4.5 square miles and extending inland 23 miles from its mouth at Newport. The tides experienced are those characteristic of the North Pacific being

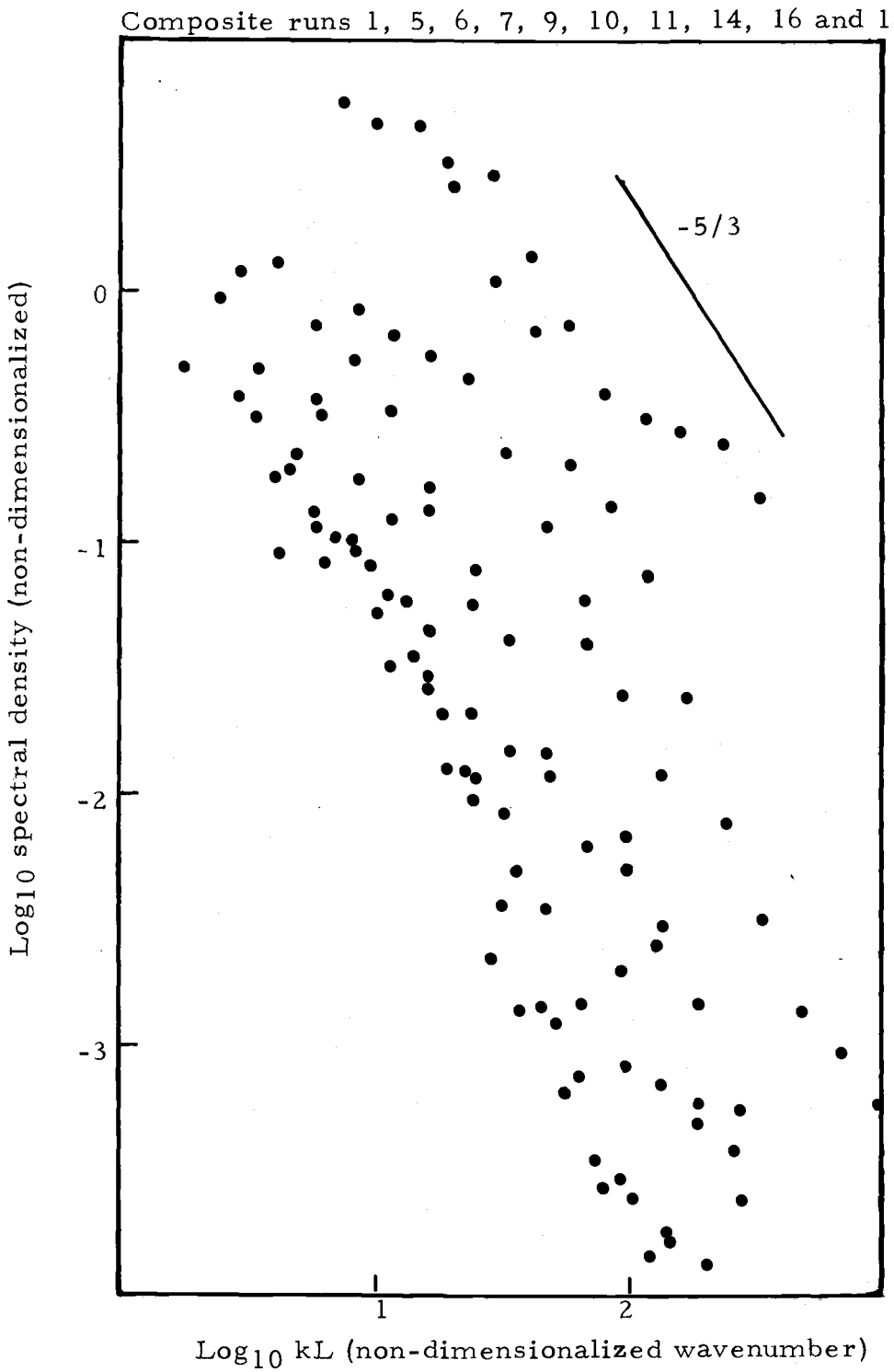

Figure 16. Normalized energy spectra.

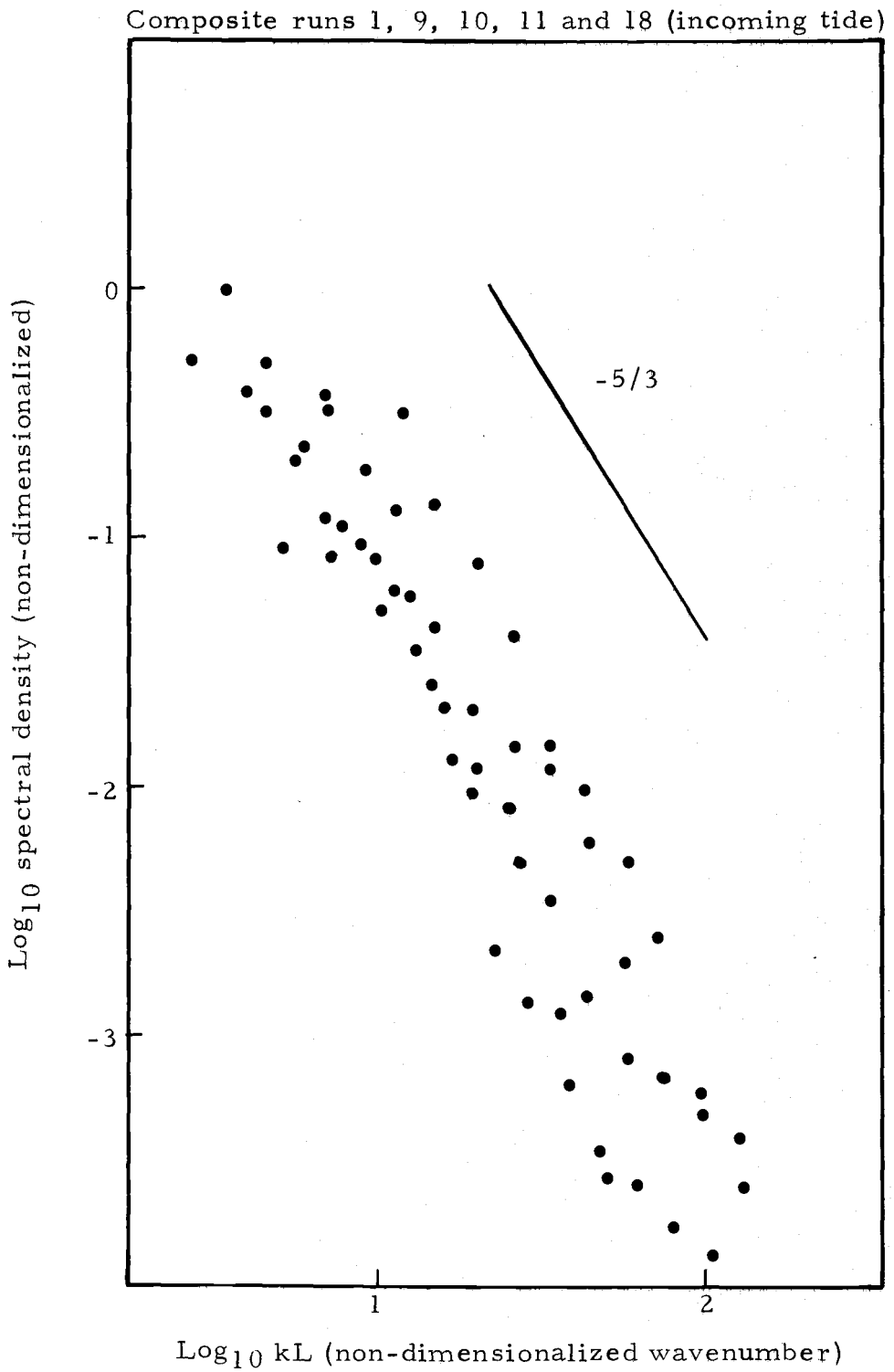

Figure 17. Non-dimensionalized energy spectra.

of the mixed semi-diurnal variety with an average tidal range of 5.5 feet. Computing the tidal prism based on this average tidal range and the surface area of the estuary from Oneatta Point seaward yields slightly less than 50 million cubic feet. A measured flow rate for the Yaquina River in late winter and early spring of 600 cubic feet per second gives a fresh water runoff of 26.8 million cubic feet during a tidal period of 44,700 seconds. The ratio of fresh water runoff to tidal prism is on the order of .2 which indicates a partly mixed estuary. This agrees with Burt and McAllister (1959) who described it as partly mixed during winter and spring and well mixed during summer and fall. The salinity data (Table 1) showed the average difference between surface and bottom salinities as 7.12 o/oo. Since the top sample bottle was 7 m above the bottom and therefore as much as 4 m below the surface, the actual average difference may have been higher. When using salinity ranges to classify an estuary, a difference in salinity from surface to bottom of less than 3 o/oo indicates a well mixed system. A difference of between 4 o/oo and 19 o/oo indicates a partly mixed system and a difference greater than 20 o/oo indicates a two layer system. In this case the salinity data also shows that the estuary was partly mixed at this time. The only times when the salinity data appear uniform (casts 4, 5, 13, 14) and allow the possibility of a well mixed system, the salinities are nearly 30 o/oo or higher. This is approximately the salinity of ocean water

which shows that these sections were practically unmixed. In these casts, the top bottle was an average of 3.3 m below the surface and probably below the layer of fresh or mixed water. Although horizontal sections were not taken during this experiment, a series was taken three months earlier in the same area. These sections (Figures A, B and C, Appendix 4) indicate that the estuary is not horizontally homogeneous. The lack of horizontal homogeneity would invalidate an attempt at a two dimensional model. This fact makes the data on particulate matter very difficult to interpret.

Water samples from each cast were analyzed for concentrations of particulate matter. Particles in ten size ranges were counted. The size ranges correspond to particles with average volumes of 11.1, 22.2, 44.4, 88.8, 178, 712, 1424, 2848, and 5696 $m^3 \times 10^{-18}$. In Table 4 can be found the amount of particulate matter at each size per cubic cm of water, for each bottle on each cast. If the water were vertically homogeneous, the concentrations of particulate matter would be the same for each sample in a given cast. Factors which can cause inhomogeneities may be classified as sources, sinks, or transfers. The surface can act as a source for wind blown material. Plankton production can occur at almost any depth within the estuary. Resuspension of bottom sediment can also be a source of particulate matter. Matter can be removed from the water column by sedimentation or by dissolving. Transfer processes in the spatial domain

Table 4. Volume of Particulate Matter per Cubic Centimeter $m^3 \times 10^{-18}$.

Mean Particle Volume ($m^3 \times 10^{-18}$)	Meters Above Bottom 7	5	3	1	Cast No.
11.1	.1887 E6	.8528 E5	.7445 E5	.6716 E5	1
22.2	.3219 E5	.7681 E5	.2879 E5	.1094 E5	
44.4	.2255 E5	.3276 E5	.2304 E5	.1074 E5	
88.8	.8853 E5	.4164 E5	.4653 E5	.2237 E5	
178	.9487 E5	.1315 E6	.1456 E6	.3613 E5	
356	.1342 E6	.3791 E6	.7476 E5	.4307 E5	
712	.7440 E5	.9362 E5	.2848 E5	.3880 E5	
1424	.3844 E5	.2278 E5	.3417 E5	.7547 E5	
2848	.4272 E5	.1993 E5	.4272 E5	.7404 E5	
5696	.1708 E5	.2278 E5	.3417 E5	.1367 E6	
11.1	.8355 E4	.1714 E6	.3212 E5	.1961 E6	2
22.2	.1844 E5	.3381 E5	.2071 E5	.3316 E5	
44.4	.1864 E5	.1123 E5	.2197 E5	.1633 E5	
88.8	.5079 E5	.3303 E5	.4502 E5	.4200 E5	
178	.5963 E5	.5357 E5	.1694 E6	.1614 E6	
356	.5980 E5	.7867 E5	.8686 E5	.1103 E6	
712	.3524 E5	.5197 E5	.2919 E5	.2919 E5	
1424	.3844 E5	.1039 E6	.4414 E5	.3417 E5	
2848	.4556 E5	.1110 E6	.3987 E5	.4841 E5	
5696	.4556 E5	.1310 E6	.5696 E5	.6835 E5	
11.1	.7196 E4	.6049 E4	.1765 E5	.1069 E5	4
22.2	.1138 E5	.5616 E4	.2115 E5	.1052 E5	
44.4	.1616 E5	.6260 E4	.2215 E5	.1385 E5	
88.8	.4582 E5	.1642 E5	.5550 E5	.4608 E5	
178	.9060 E5	.5286 E5	.9416 E5	.1317 E6	
356	.5660 E5	.6728 E5	.7155 E5	.1772 E6	
712	.4378 E5	.2954 E5	.7618 E5	.8828 E5	
1424	.3132 E5	.4556 E5	.7974 E5	.7547 E5	
2848	.3132 E5	.5411 E5	.6265 E5	.9398 E5	
5696	.3987 E5	.5696 E5	.7974 E5	.6835 E5	
11.1	.2150 E6	.2761 E5	.2705 E5	.3988 E5	5
22.2	.2872 E5	.1125 E5	.1141 E5	.6060 E4	
44.4	.1482 E5	.9990 E4	.8835 E4	.6393 E4	
88.8	.3542 E5	.3285 E5	.3436 E5	.3196 E5	
178	.6230 E5	.9078 E5	.6336 E5	.4343 E5	
356	.9184 E5	.4450 E5	.5446 E5	.5268 E5	
712	.8010 E5	.3061 E5	.3310 E5	.5375 E5	
1424	.1281 E6	.4129 E5	.2848 E5	.3844 E5	
2848	.6550 E5	.6550 E5	.2848 E5	.4841 E5	
5696	.5696 E5	.6265 E5	.5696 E5	.4556 E5	

(Continued on next page)

Table 4. (Continued)

Mean Particle Volume ($m^3 \times 10^{-18}$)	Meters Above Bottom 7	5	3	1	Cast No.
11.1	.2347 E6	.1251 E5	.2477 E5	.2214 E5	6
22.2	6346 E5	.1032 E5	.1491 E5	.1640 E5	
44.4	.1611 E5	.1434 E5	.1216 E5	.2326 E5	
88.8	.4715 E5	.4582 E5	.5683 E5	.7725 E5	
178	.6105 E5	.1069 E6	.7458 E5	.1256 E6	
356	.1391 E6	.7404 E5	.9006 E5	.2474 E6	
712	.1448 E6	.1078 E6	.8864 E5	.1911 E6	
1424	.1110 E6	.1523 E6	.1324 E6	.1509 E6	
2848	.1196 E6	.2079 E6	.1737 E6	.1936 E6	
5696	.1594 E6	.1480 E6	.1708 E6	.1767 E6	
11.1	.2613 E5	.1463 E5	.1671 E6	.1539 E5	7
22.2	2619 E5	.2910 E5	.7026 E5	.1813 E5	
44.4	.4013 E5	.4337 E5	.2228 E5	.2220 E5	
88.8	.7645 E5	.1239 E6	.9137 E5	.7627 E5	
178	.1057 E6	.1886 E6	.1548 E6	.1219 E6	
356	.1242 E6	.1893 E6	.2210 E6	.2559 E6	
712	.1153 E6	.1384 E6	.1470 E6	.1908 E6	
1424	.1424 E6	.1011 E6	.1723 E6	.1922 E6	
2848	.9113 E5	.6550 E5	.1651 E6	.2506 E6	
5696	.6265 E5	.3987 E5	.2050 E6	.1310 E6	
11.1	.4646 E5	.4813 E5	.1789 E5	.6099 E5	8
22.2	.3767 E5	.3827 E5	.2191 E5	.9923 E4	
44.4	.4111 E5	.3396 E5	.3201 E5	.1416 E5	
88.8	.1006 E6	.7148 E5	.7778 E5	.3996 E5	
178	.1425 E6	.1247 E6	.1130 E6	.5393 E5	
356	.1591 E6	.9505 E5	.8935 E5	.6621 E5	
712	.1014 E6	.7582 E5	.9754 E5	.7155 E5	
1424	.7974 E5	.7404 E5	.1281 E6	.8259 E5	
2848	.4272 E5	.4272 E5	.7974 E5	.1167 E6	
5696	.2848 E5	.5126 E5	.8544 E5	.7404 E5	
11.1	.6433 E5	.5451 E5	.6648 E5	.8644 E4	9
22.2	.2606 E5	.2348 E5	.2493 E5	.8258 E4	
44.4	.4542 E5	.1522 E5	.4923 E5	.9235 E4	
88.8	.1493 E6	.3472 E5	.1513 E6	.2548 E5	
178	.1902 E6	.5767 E5	.1740 E6	.3666 E5	
356	.1270 E6	.6372 E5	.2477 E6	.4022 E5	
712	.1929 E6	.1014 E6	.3399 E6	.5268 E5	
1424	.1723 E6	.5838 E5	.2662 E6	.8971 E5	
2848	.1338 E6	.4272 E5	.3047 E6	.1025 E6	
5696	.1253 E6	.4556 E5	.2221 E6	.8544 E5	

(Continued on next page)

Table 4. (Continued)

Mean Particle Volume ($m^3 \times 10^{-18}$)	Meters Above Bottom 7	5	3	1	Cast No.
11.1	.3060 E5	.1571 E5	.1825 E5	.1092 E6	10
22.2	.2861 E5	.2601 E5	.2120 E5	.2719 E5	
44.4	.6957 E5	.7445 E5	.2499 E5	.4022 E5	
88.8	.1936 E6	.1815 E6	.5017 E5	.6393 E5	
178	.1927 E6	.2386 E6	.4432 E5	.5696 E5	
356	.1886 E6	.1993 E6	.7796 E5	.4200 E5	
712	.3179 E6	.3332 E6	.1082 E6	.2164 E6	
1424	.2492 E6	.3204 E6	.2990 E5	.9540 E5	
2848	.1537 E6	.2363 E6	.2848 E5	.1167 E6	
5696	.7974 E5	.2164 E6	.2278 E5	.1139 E5	
11.1	.2162 E5	.8089 E5	.2234 E5	.2801 E5	11
22.2	.3865 E5	.8171 E5	.2051 E5	.3225 E5	
44.4	.5905 E5	.9075 E5	.2894 E5	.3880 E5	
88.8	.1221 E6	.1771 E6	.6553 E5	.9670 E5	
178	.7404 E5	.1133 E6	.7974 E5	.1425 E6	
356	.9149 E5	.1384 E6	.1310 E6	.2168 E6	
712	.1274 E6	.2004 E6	.1384 E6	.2801 E6	
1424	.9540 E5	.1566 E6	.1780 E6	.3503 E6	
2848	.1224 E6	.2079 E6	.2079 E6	.3047 E6	
5696	.6265 E5	.1253 E6	.2449 E6	.2961 E6	
11.1	.4082 E5	.4010 E5	.2396 E5	.3824 E5	13
22.2	.1332 E5	.1718 E5	.2817 E5	.2124 E5	
44.4	.1141 E5	.9812 E4	.3862 E5	.4590 E5	
88.8	.2921 E5	.2442 E5	.1134 E6	.4839 E5	
178	.4806 E5	.3417 E5	.1632 E6	.7298 E5	
356	.7440 E5	.6301 E5	.2584 E6	.1477 E6	
712	.6514 E5	.7867 E5	.2438 E6	.1925 E6	
1424	.4984 E5	.1082 E6	.2591 E6	.2862 E6	
2848	.5980 E5	.1765 E6	.2762 E6	.3161 E6	
5696	.8544 E5	.1936 E6	.2791 E6	.3018 E6	
11.1	.2113 E6	.2698 E5	.3474 E5	.3215 E5	14
22.2	.7987 E5	.1607 E5	.1709 E5	.1984 E5	
44.4	.3108 E5	.2557 E5	.2015 E5	.2037 E5	
88.8	.5141 E5	.6189 E5	.4422 E5	.6029 E5	
178	.6621 E5	.1035 E6	.7244 E5	.8775 E5	
356	.1167 E6	.1470 E6	.1577 E6	.1441 E6	
712	.1146 E6	.1388 E6	.1470 E6	.1854 E6	
1424	.1751 E6	.2221 E6	.2235 E6	.2776 E6	
2848	.1851 E6	.2164 E6	.1879 E6	.2933 E6	
5696	.2107 E6	.1594 E6	.2164 E6	.2677 E6	

(Continued on next page)

Table 4. (Continued)

Mean Particle Volume ($m^3 \times 10^{-18}$)	Meters Above Bottom 7	5	3	1	Cast No.
11.1	.1003 E6	.1375 E6	.3023 E5	.5636 E5	15
22.2	.3580 E5	.2681 E5	.1063 E5	.1707 E5	
44.4	.2695 E5	.2046 E5	.1602 E5	.1811 E5	
88.8	.5550 E5	.5496 E5	.3596 E5	.4146 E5	
178	.7351 E5	.3435 E5	.6639 E5	.3916 E5	
356	.8330 E5	.3844 E5	.9469 E5	.5233 E5	
712	.8935 E5	.4094 E5	.1213 E6	.3809 E5	
1424	.6123 E5	.4984 E5	.1509 E6	.3560 E5	
2848	.5696 E5	.7974 E5	.1480 E6	.4272 E5	
5696	.6265 E5	.3417 E5	.1993 E6	.6265 E5	
11.1	.1874 E6	.3210 E5	.2446 E5	.1203 E5	16
22.2	.1007 E6	.1571 E5	.9079 E4	.5439 E4	
44.4	.4302 E5	.3325 E5	.2326 E5	.1074 E5	
88.8	.8675 E5	.1039 E6	.8951 E5	.3809 E5	
178	.1078 E6	.9754 E5	.8170 E5	.6087 E5	
356	.1260 E6	.1530 E6	.8437 E5	.9683 E5	
712	.1772 E6	.1648 E6	.9647 E5	.1181 E6	
1424	.1865 E6	.1210 E6	.9256 E5	.1367 E6	
2848	.1338 E6	.1196 E6	.1082 E6	.1224 E6	
5696	.9113 E5	.5126 E5	.1253 E6	.9113 E5	
11.1	.1029 E6	.7003 E5	.2085 E5	.2174 E5	17
22.2	.4557 E5	.3503 E5	.3427 E5	.2521 E5	
44.4	.5714 E5	.6247 E5	.3698 E5	.3547 E5	
88.8	.1639 E6	.1457 E6	.5754 E5	.5274 E5	
178	.2127 E6	.1863 E6	.8561 E5	.5055 E5	
356	.2673 E6	.1893 E6	.9647 E5	.6870 E5	
712	.2516 E6	.1990 E6	.9149 E5	.8223 E5	
1424	.1580 E6	.1424 E6	.1039 E6	.1153 E6	
2848	.1623 E6	.1338 E6	.9683 E5	.1424 E6	
5696	.1310 E6	.9683 E5	.7974 E5	.8544 E5	
11.1	.3792 E6	.1668 E6	.4647 E5	.1540 E6	18
22.2	.9521 E6	.8318 E5	.4435 E5	.5352 E5	
44.4	.1463 E7	.3152 E5	.6295 E5	.2180 E5	
88.8	.4431 E5	.6056 E5	.1682 E6	.5283 E5	
178	.3275 E5	.7155 E5	.2127 E6	.4752 E5	
356	.2420 E5	.1053 E6	.2420 E6	.6692 E5	
712	.3061 E5	.1569 E6	.2534 E6	.9718 E5	
1424	.3417 E5	.2050 E6	.2107 E6	.1552 E6	
2848	.4272 E5	.2306 E6	.1651 E6	.2392 E6	
5696	.3417 E5	.2221 E6	.1708 E6	.3246 E6	

include horizontal and vertical advection and diffusion. Within the size ranges transfer can occur by fragmentation, solution, or flocculation. The above list is by no means exhaustive. Obviously, it was beyond the scope of this experiment to evaluate the entire scheme which determines the particle size distribution. However, with the data collected, some inferences about the processes can be made. The average concentration of particulate matter in the sizes measured was computed for each cast. An increase in the average concentration could indicate an increase in the strength of a source or the decrease in the strength of a sink. Multilinear regression analysis was performed comparing the above average to the following parameters:

U the mean velocity

$\mu = ((1/3)(u_i u_i))^{1/2}$ the turbulent velocity scale

$||\tau_{ij}||$ = the norm of the Reynolds' stress tensor

$||\tau_{i2}||$ = the norm of the cross stream component of τ_{ij}

$||\tau_{i3}||$ = the norm of the vertical component of τ_{ij}

In addition, the base ten logarithm of the last three parameters were used in the regression analysis. Since the number of factors which affect the average concentration is large and many are not included in the analysis, it was not expected that a large correlation between the average and any of the individual parameters exist. The most significant correlations with average concentration were with $\log_{10}||\tau_{ij}||$ and $\log_{10}||\tau_{i3}||$. The correlation coefficients were .533

and .519, respectively. The regression model constructed using these parameters was:

$$\text{ave. concentration} \times 10^{-6} = 1.146 + 2.9535 \log_{10} ||\tau_{ij}|| - 2.6509 \log_{10} ||\tau_{i3}||$$

This model accounted for over 60 percent of the variability in the average concentration. More information is necessary before it can be determined if the correlation found here represents a causal relationship among the parameters, and what precisely that relation might be. One suggestion is that the Reynolds stress tensor is an indication of the ability of the flow to resuspend bottom sediment. This would account for the positive coefficient, since increased resuspension would increase the concentration. Likewise, the negative coefficient for $\log_{10} ||\tau_{i3}||$ would be explained if that quantity was indicative of the amount of vertical diffusion. Increasing vertical diffusion would lower the concentrations. Rigorous testing of these possibilities could prove to be an interesting and informative project.

If the bottom is considered as a source of particulate matter, a closer look at the bottom section of the water column might be in order. The average coefficient of variation in the concentration of suspended matter contained in the bottom two bottles was computed. This was done by averaging the coefficient of variation for each size range measured. The coefficient of variation is a measure of the inhomogeneity of the water. The larger the coefficient, the less

homogeneous the water is. The linear regression model constructed using this as the dependent variable was the following:

$$\text{ave. coeff. of variation} = 7.1162 + .42849\,U + 21.137 \log_{10}||\tau_{ij}|| - 20.769 \log_{10}||\tau_{i3}|| .$$

This model accounted for over half of the variability in the average coefficient of variation. Obviously, the model is not deterministic, but it is reasonable and does shed some light on the problem. Increasing the mean velocity results in a greater capability of the flow to suspend particulate matter. If this increase occurs only near the bottom, it will increase the inhomogeneity of the water column. This accounts for the positive coefficient. As in the previous model, an increase in Reynolds' stress may result in increased resuspension of bottom sediment. If this is not propagated upward throughout the water column, it will result in increased inhomogeneity. Again this is indicated by the positive coefficient. If the particulate matter is diffused vertically, by an increased vertical component of the Reynolds' stress, then the inhomogeneity will decrease. The negative coefficient is consistent with this. As was stated before, the rigorous investigation of these possibilities could be rewarding.

VII. CONCLUSIONS

The three component drag probe was shown to be an effective instrument for measuring certain ranges of turbulent spectra. Parameters which depend on all three components of motion like E(k) which previously could only be inferred from one dimensional spectra after assuming isotropy, can now be measured directly over ranges of k. Spectra in the range of smaller wavenumbers are thought to be dependent on the local geometry. In this experiment F(kL) was calculated for wavenumbers outside the predicted inertial subrange. When the base 10 logarithm of F(kL) was plotted against the base 10 logarithm of (kl) a least squares fit line has a slope of approximately -5/3. This indicated spectral behavior like that in the inertial subrange even when the local strain rate was less than an order of magnitude greater than the mean rate of strain. In its present configuration, the size of the probe head and its mechanical frequency response characteristics limit the range of wavenumbers which can be satisfactorily measured. At present 10 Hz is about the limit of good reliability, based on laboratory testing procedure described by Earle (1971). The good agreement of measured data with theoretical predictions adds to the confidence in the measurements. There is nothing in the design of the probe head which prohibits its size from being reduced. If this were done and the frequency response characteristics of the system enhanced, the range of wavenumbers over

which the instrument measures effectively could be greatly increased. On the other end of the spectra, the addition of an Analog to Digital conversion capabilities and a recording system with a computer compatible output would increase the length of record which could be handled without prohibitively increasing the cost of the data processing. The manual digitizing of the oscillograph records limited from both a time and cost standpoint the length of record which could be effectively handled. This in turn limited the capability of measuring low frequency (small wavenumber) spectra.

If the data conversion problem were handled more efficiently, it would allow for the positioning of an array of these instruments which could add information about quantities like $\partial u/\partial x$, $\partial v/\partial y$ and $\partial w/\partial z$ in addition to the u, v and w, now measured directly and $\partial u/\partial x$ which is inferred using Taylor's Hypothesis.

The last section may not have answered any questions on its own. Perhaps its value is that it illustrates some of the problems involved in the examination of suspended particulate matter in the estuarine environment and points to some new considerations in the problem of mixing. The information about the turbulent characteristics of estuarine flow which are now accessible to the researcher as a result of the development and refinement of the three component drag probe for this purpose can shed considerable light on the structure of the turbulent flows and its relation to mixing and other

questions. This experiment was in the nature of opening a door previously locked. The full exploitation of this instrument for research purposes still remains ahead.

BIBLIOGRAPHY

Burt, W. V., and W. B. McAlister. 1959. Recent studies in the hydrography of Oregon estuaries. Res. Briefs, Fish Comm. of Oregon, 7:14-27.

Draper, N. R., and H. Smith. 1966. Applied regression analysis. New York, John Wiley & Sons, Inc. 407 p.

Earle, M. D. 1971. A three component drag probe for the measurement of ocean wave orbital velocities and turbulent water velocity fluctuations. Ph. D. Thesis. Oregon State University, Corvallis, Oregon.

Earle, M. D., J. H. Groelle, G. F. Beardsley, Jr. 1970. A three component drag probe for the measurement of turbulent water velocity fluctuations. Review of Scientific Instruments 41:1021-1025.

Fischer, H. B. 1972. Mass transport mechanisms in partially stratified estuaries. J. Fluid Mech. vol. 53 part 4 pp. 671-687.

Gear, C. W. 1971. Numerical initial value problems in ordinary differential equations. Englewood Cliffs, N. J. Prentice-Hall, Inc. 253 p.

Grant, H. L., R. W. Stewart and A. Moilliet. 1962. Turbulence spectra from a tidal channel. J. Fluid Mech. 12:241-268.

Groen, P. 1967. On the residual transport of suspended matter by an alternating tidal current. Neth. J. Sea Res. 3, 4, p. 564-574.

Hinze, J. O. 1959. Turbulence. New York, McGraw-Hill. 586 p.

Ippen, A. T., (ed.). 1966. Estuary and coastline hydrodynamics. New York, McGraw-Hill. 744 p.

Kulm, L. D., and J. V. Byrne. 1967. Sediments in Yaquina Bay Oregon. In: Estuaries, American Association for the Advancement of Science, Washington, D. C. 226-238.

Lin, C. C. 1961. Statistical theories of turbulence. Princeton, N.J. Princeton University Press. 60 p.

Postma, H. 1967. Sediment transport and sedimentation in the estuarine environment. In: Estuaries, American Association for the Advancement of Science, Washington, D. C. 158-179.

Sakamoto, W. 1972. Study on the process of river suspension from flocculation to accumulation in estuary. Bulletin of the Ocean Research Institute, University of Tokyo, No. 5, October. 46 p.

Schubel, J. R. 1969. Size distributions of the suspended particles of the Chesapeake Bay turbidity maximum. Neth. J. Sea Res. 4(3):283-309.

Tennekes, H., and J. L. Lumley. 1972. A first course in turbulence. Cambridge, Mass. M.I.T. Press. 300 p.

APPENDICES

APPENDIX 1

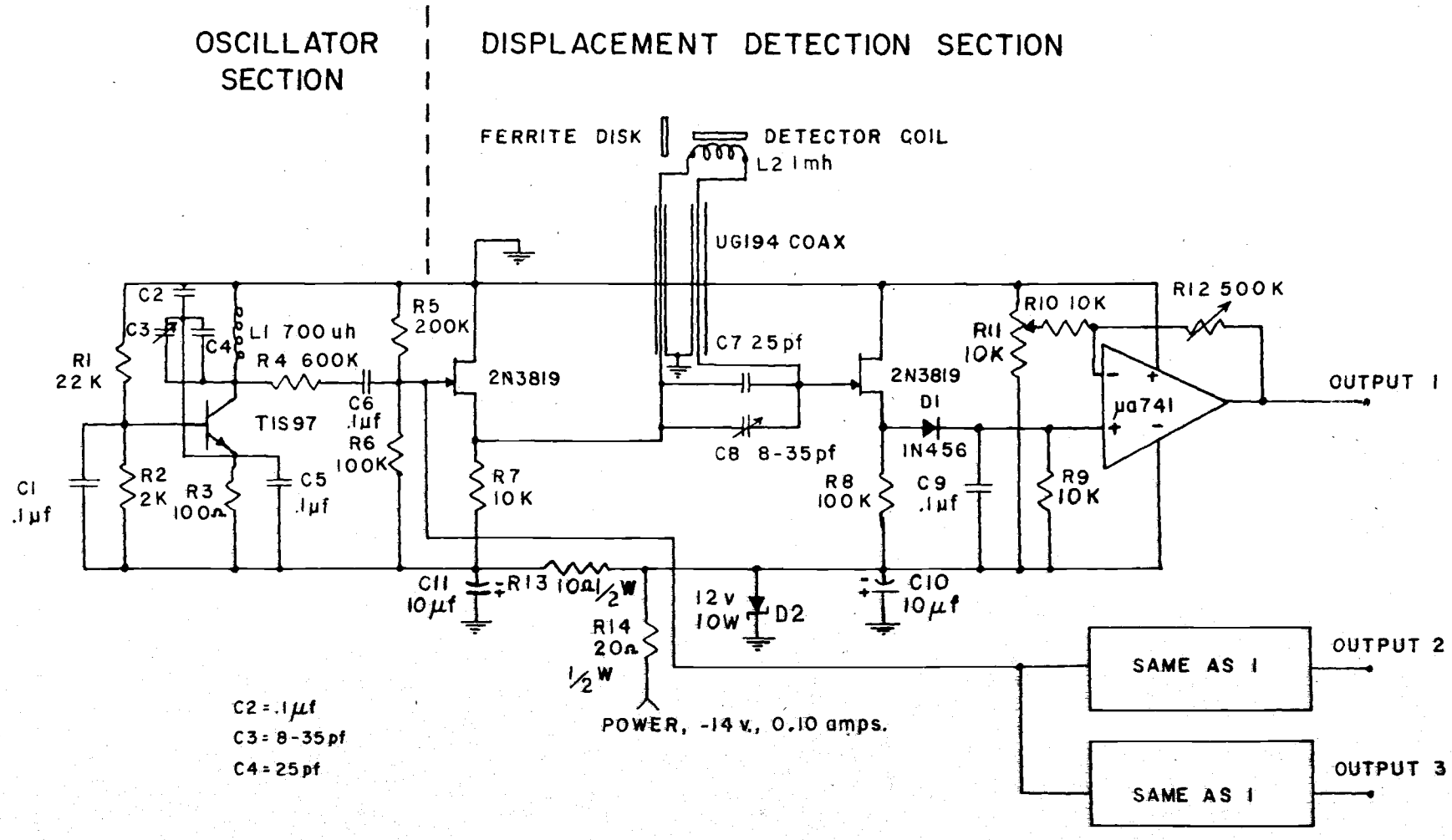

Figure A. Drag probe electronics.

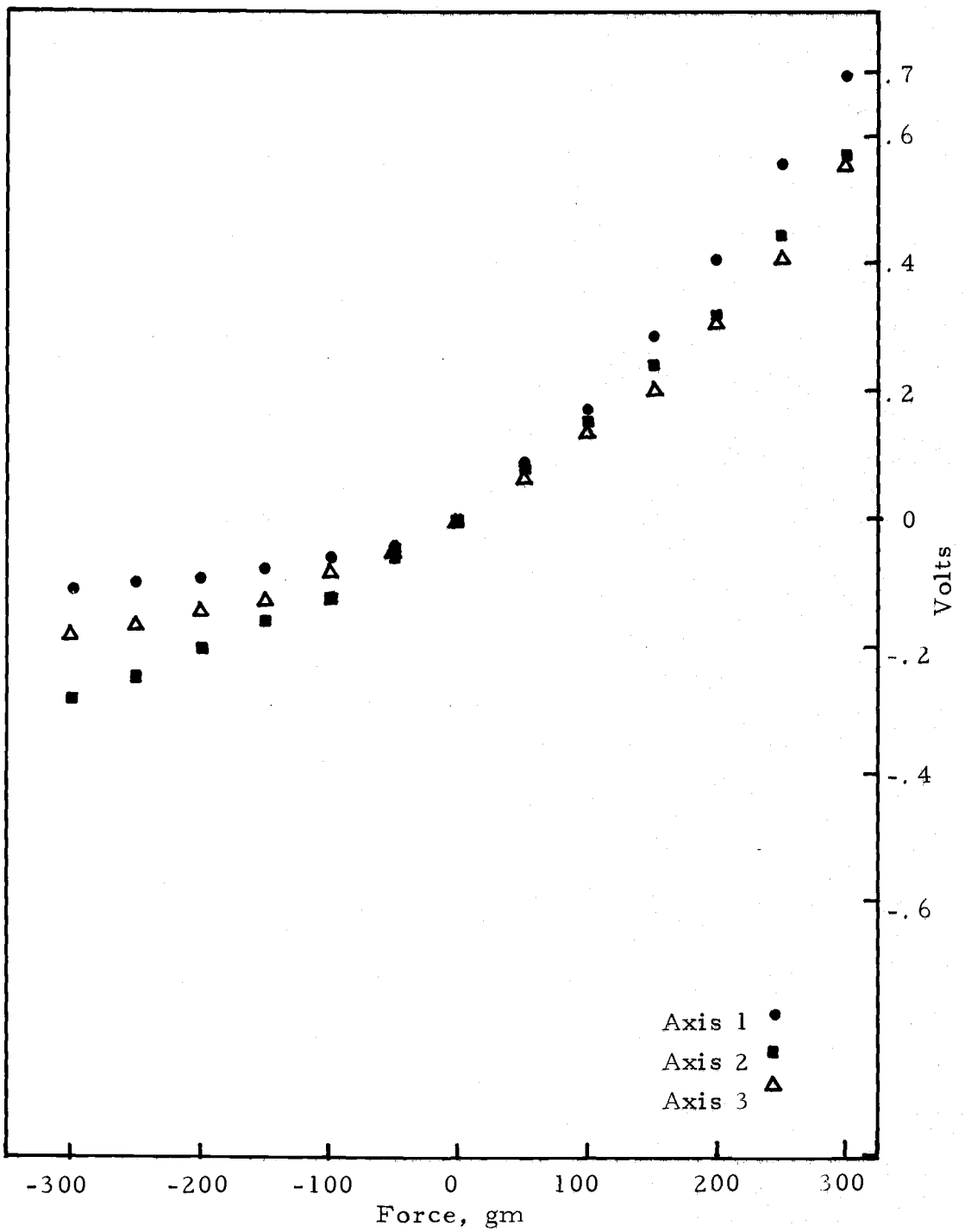

Figure B. Drag probe calibration curves.

APPENDIX 2

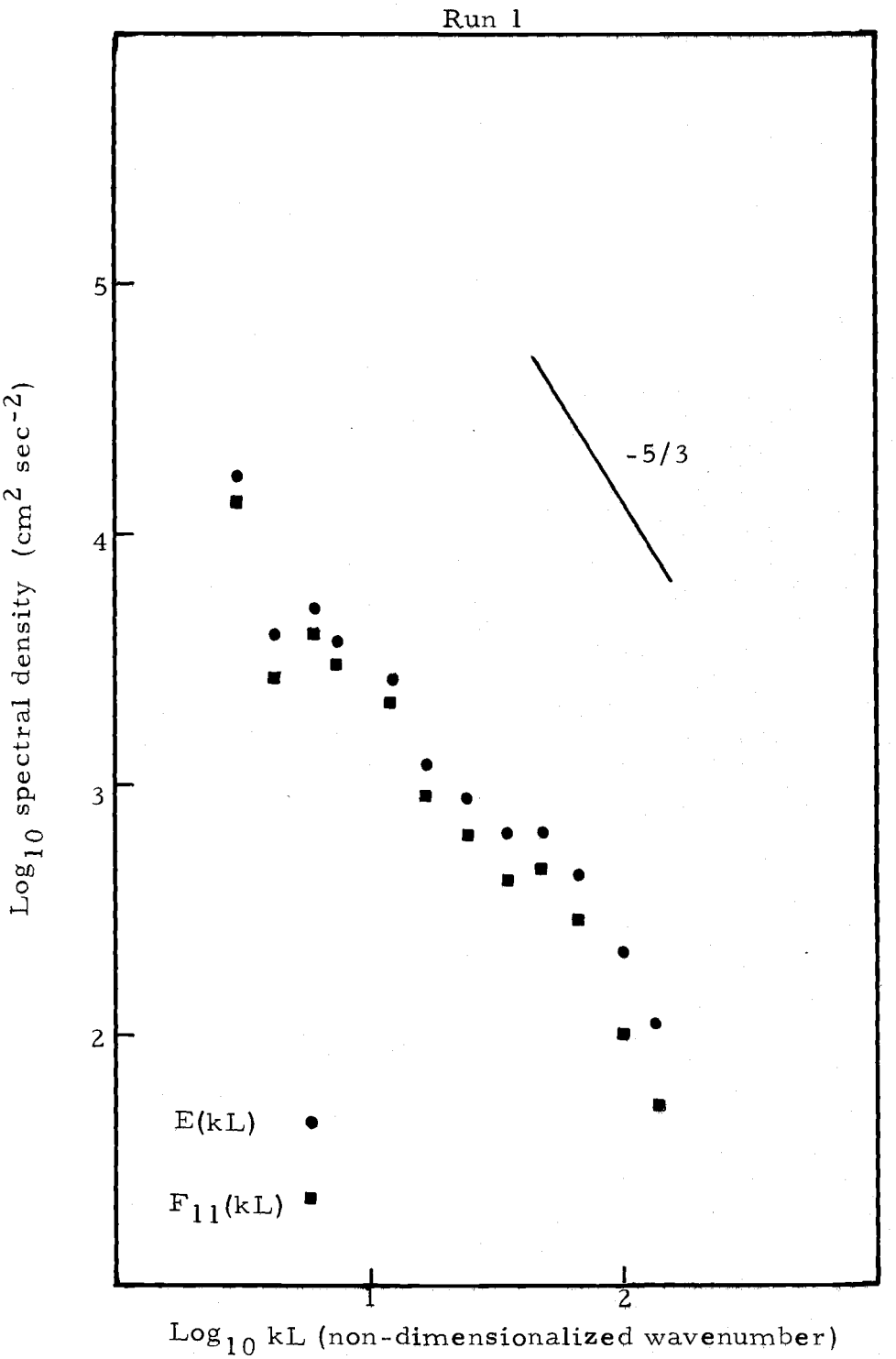

Figure A. Energy spectra.

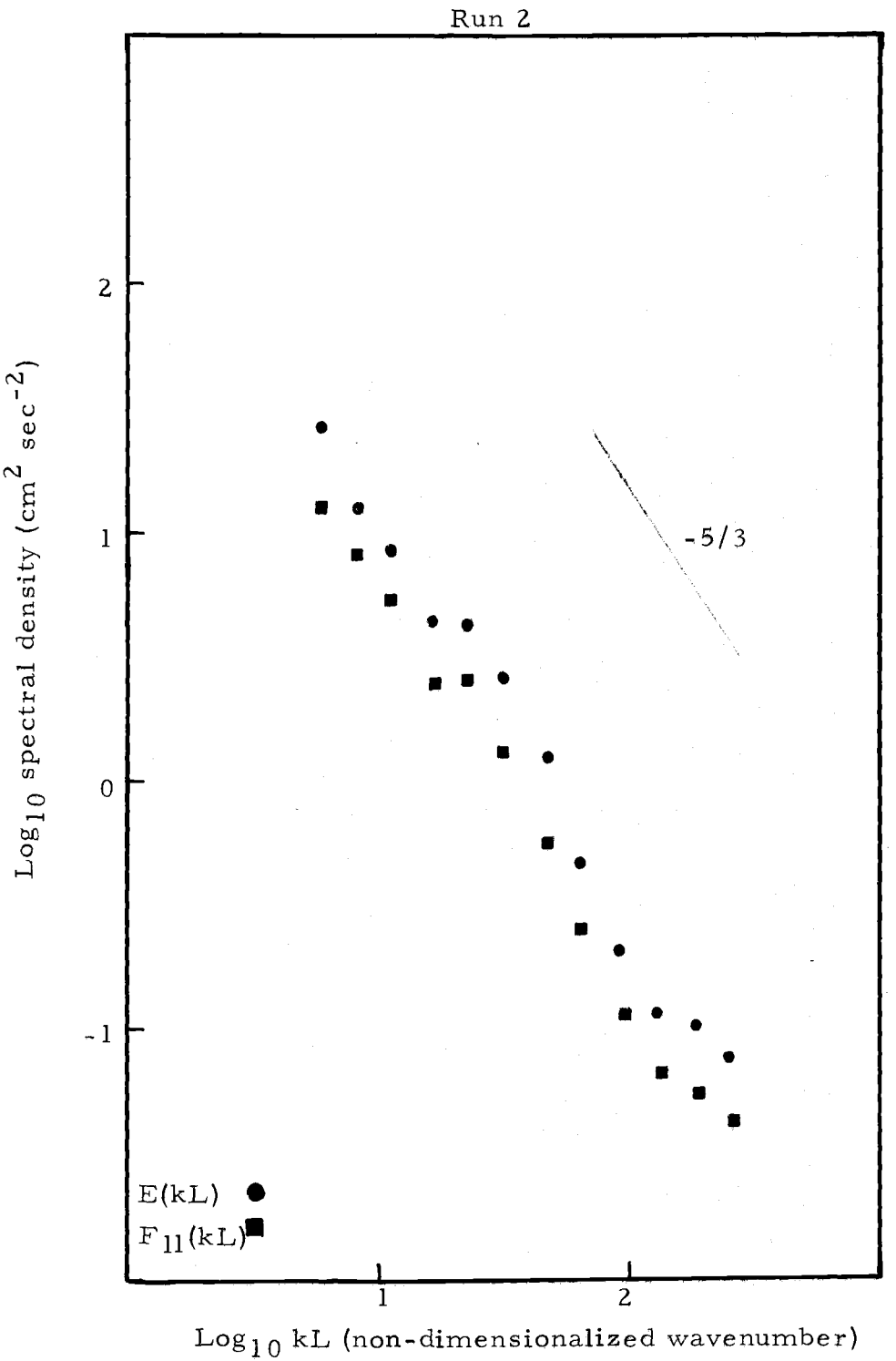

Figure B. Energy spectra.

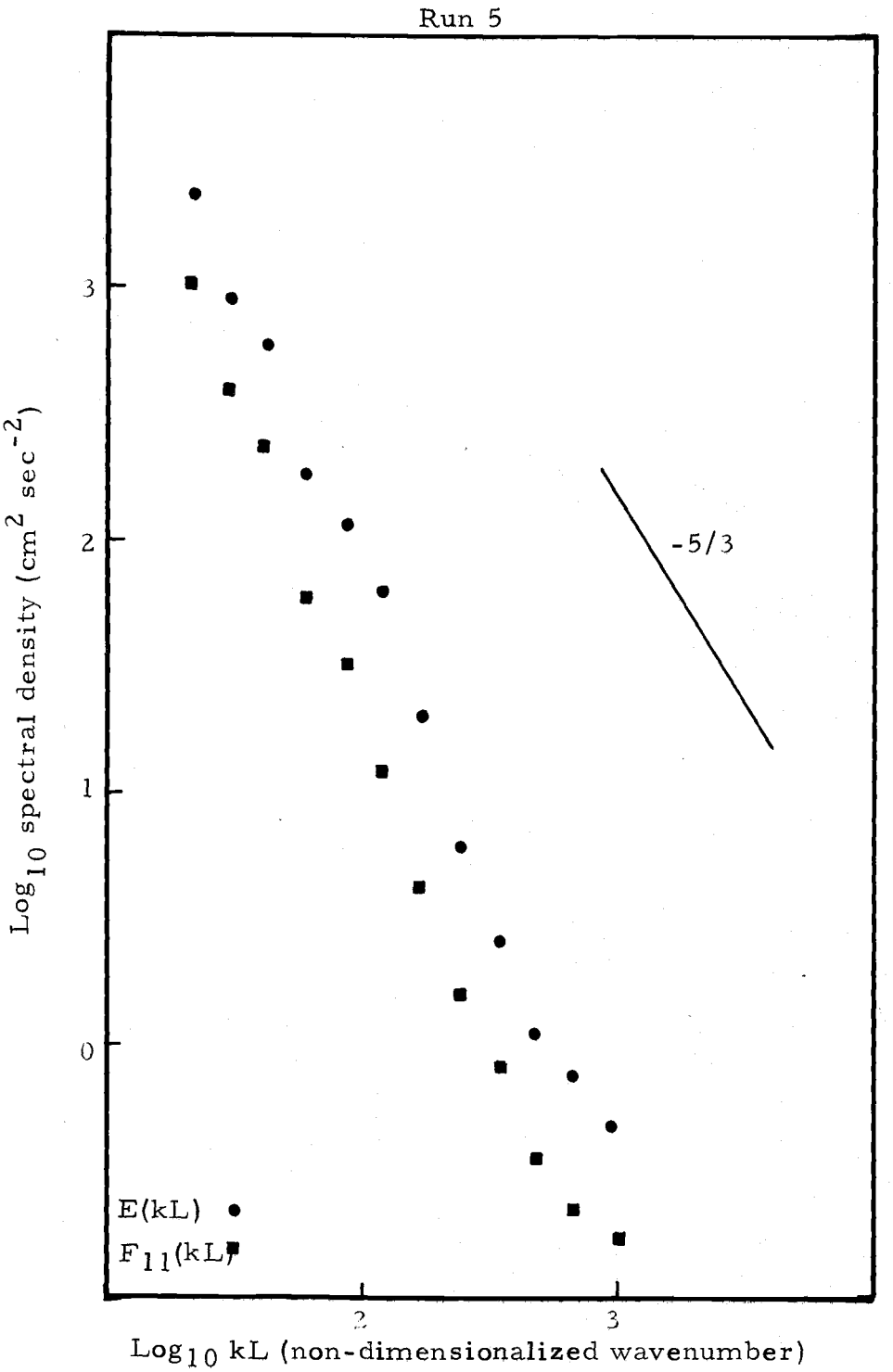

Figure C. Energy spectra.

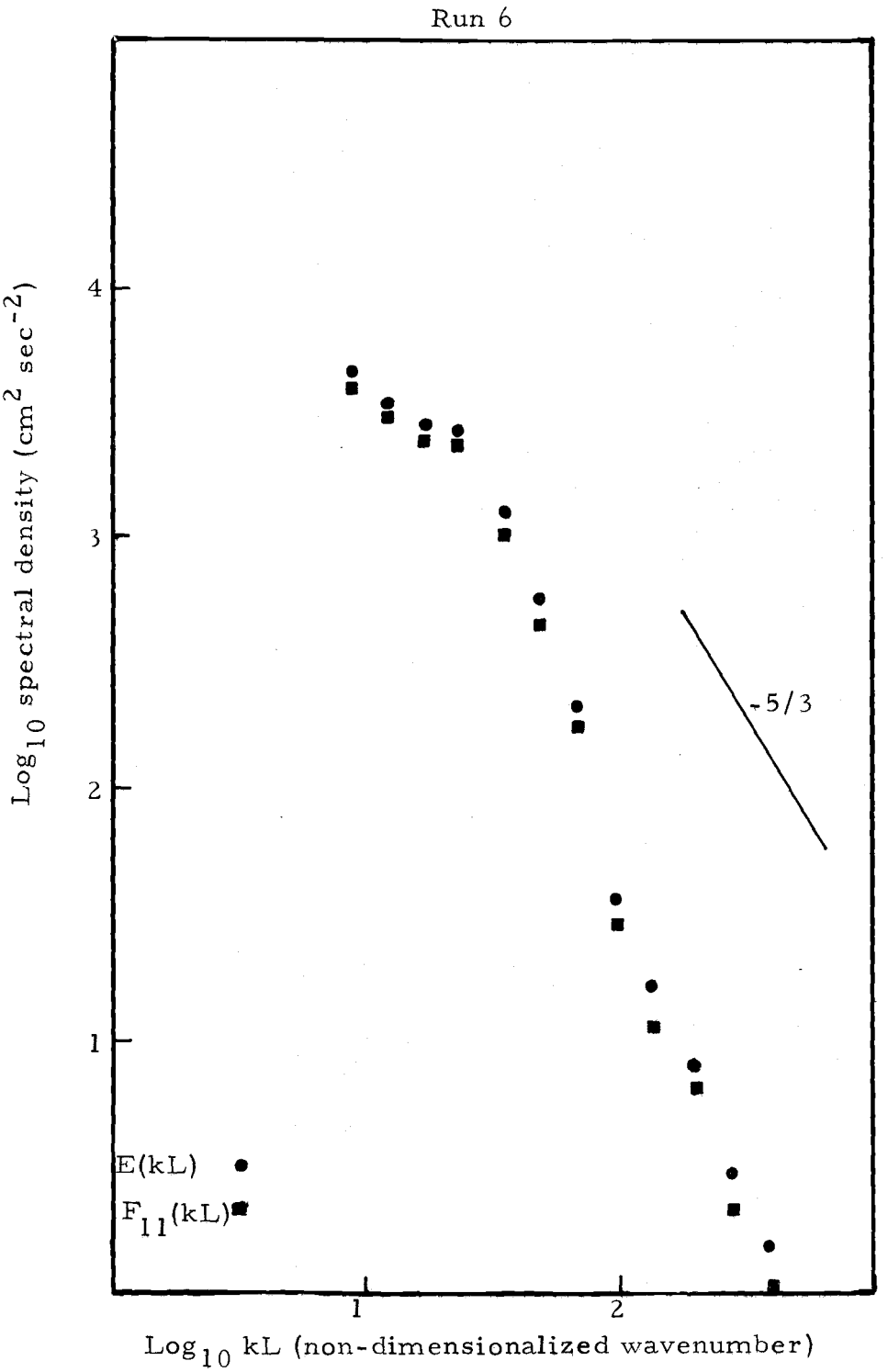

Figure D. Energy spectra.

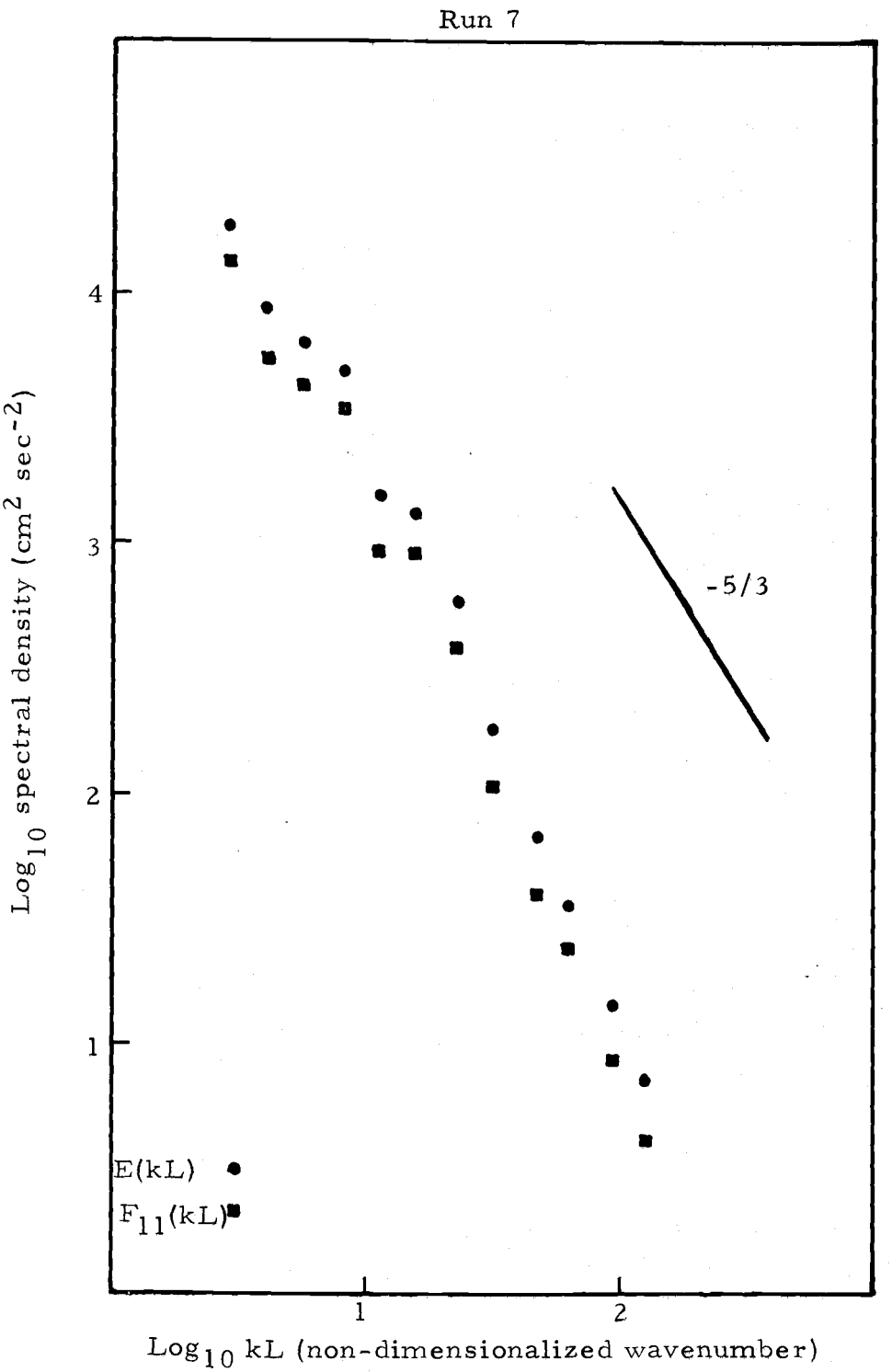

Figure E. Energy spectra.

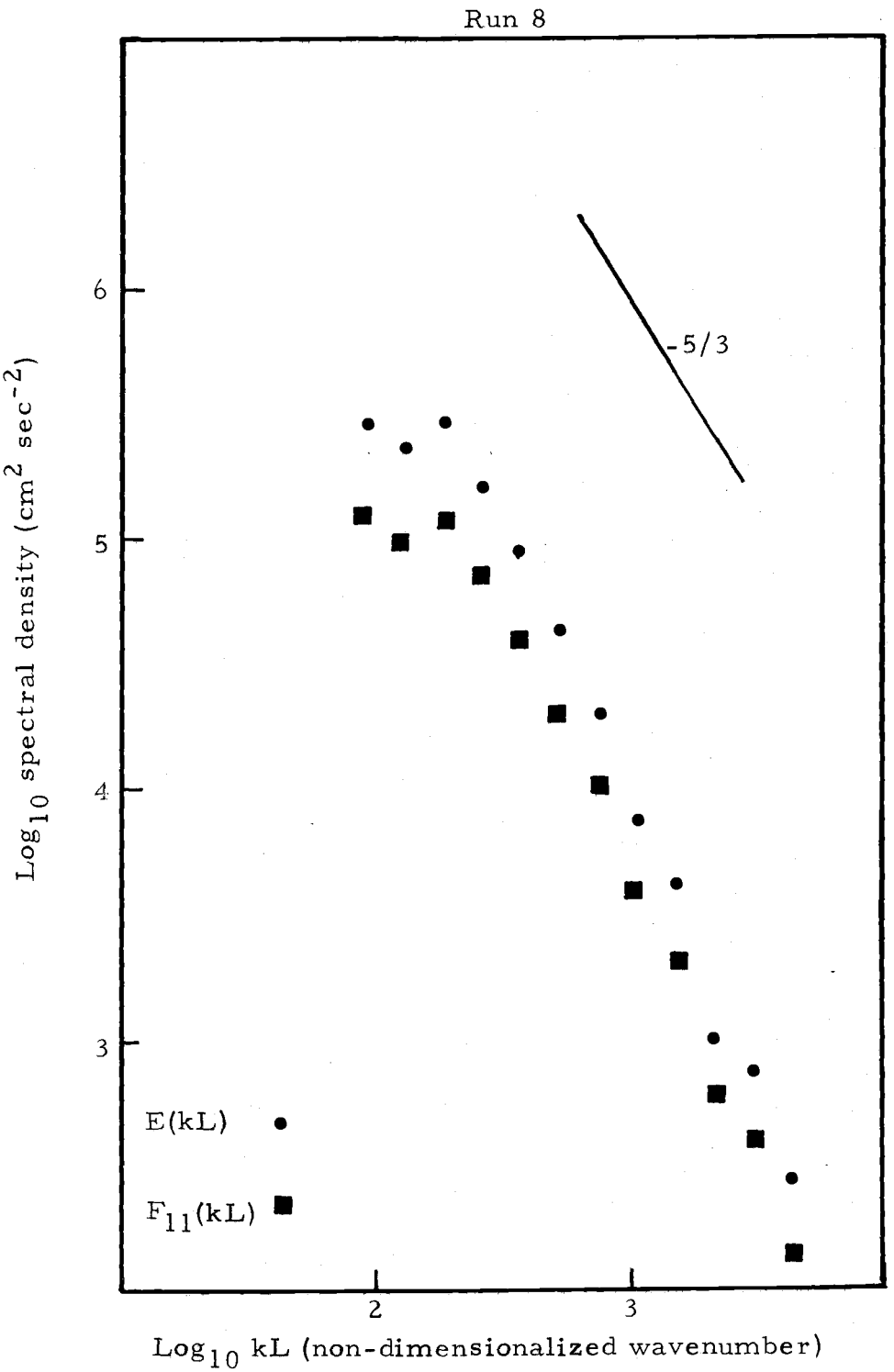

Figure F. Energy spectra.

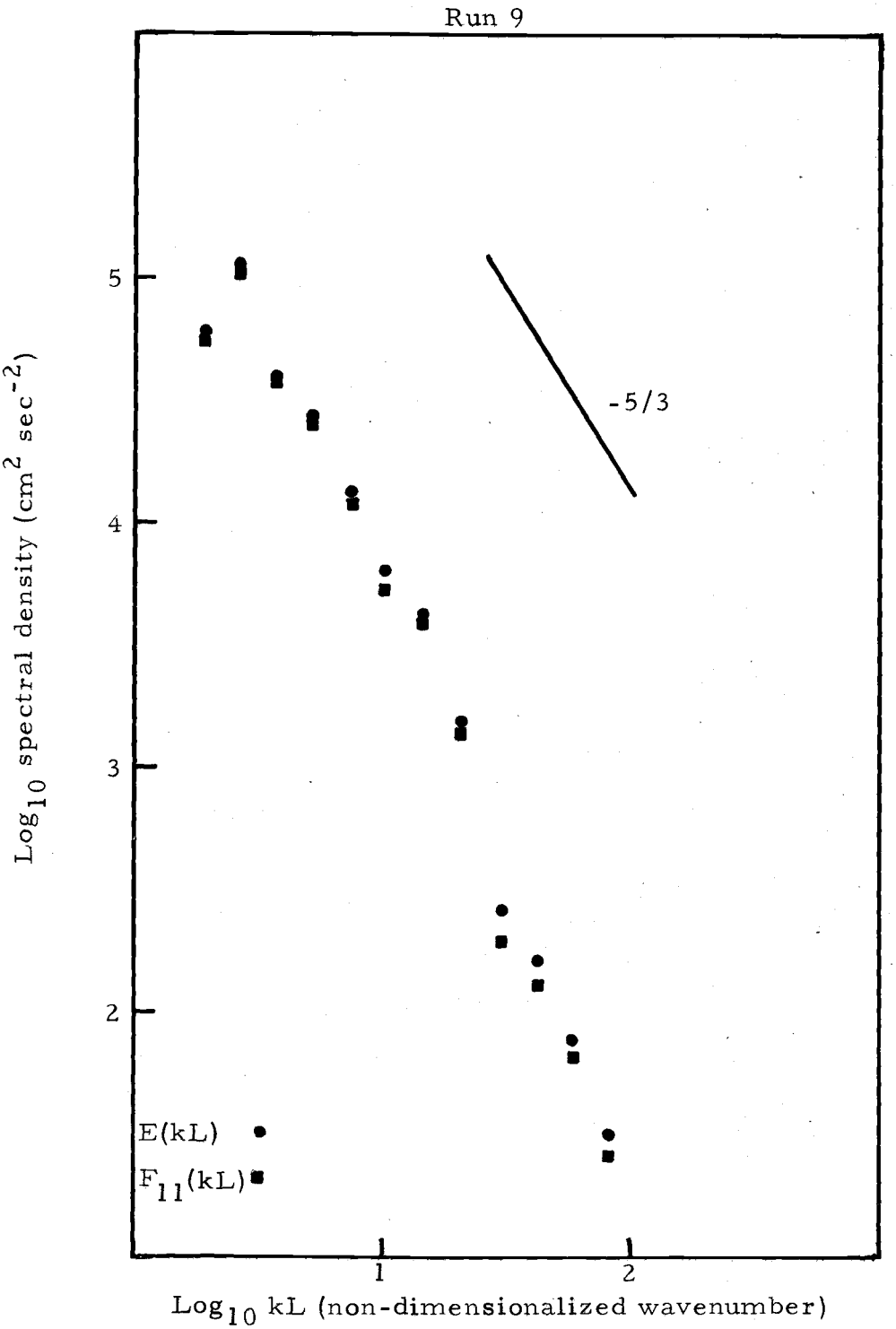

Figure G. Energy spectra.

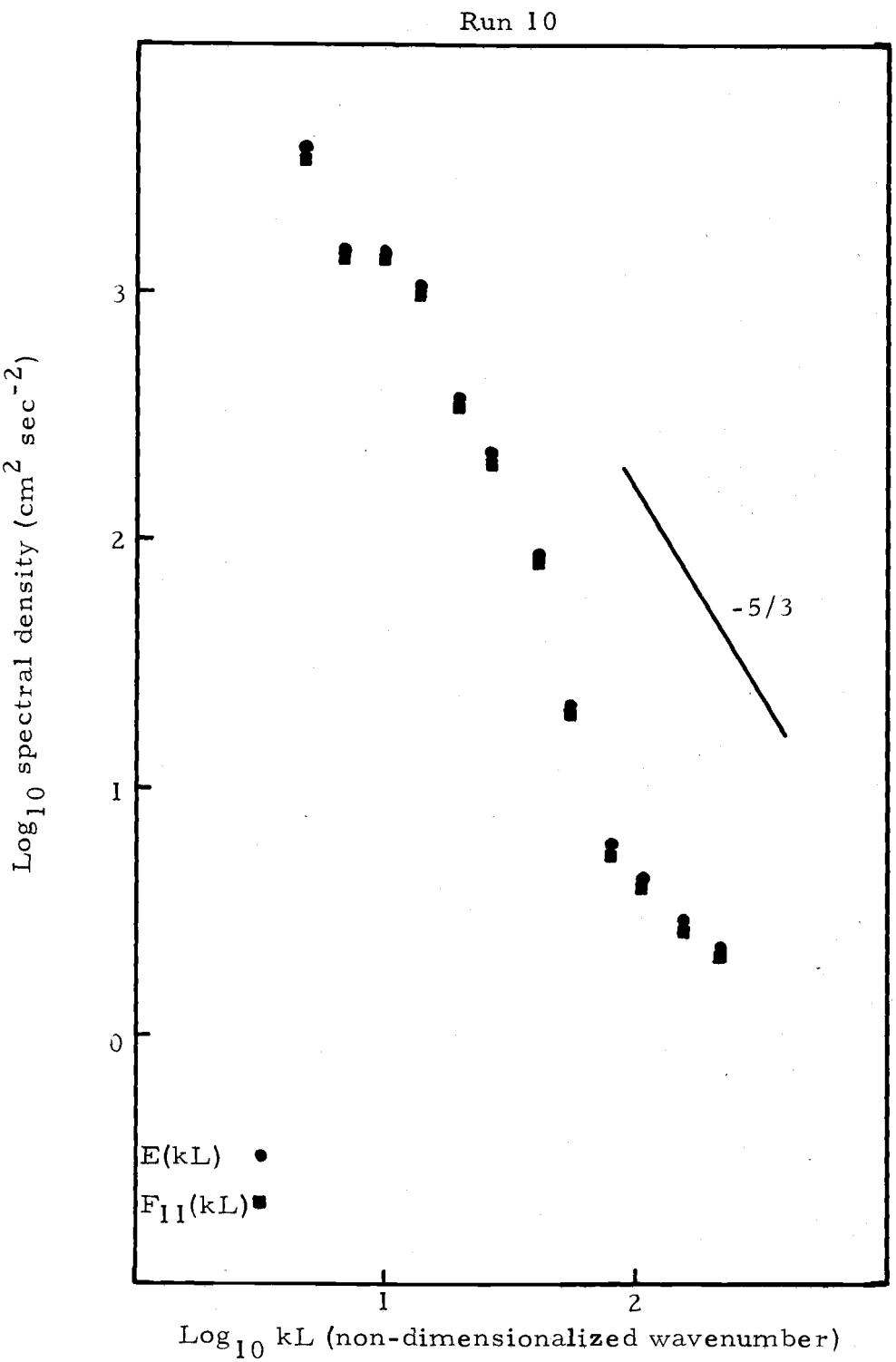

Figure H. Energy spectra.

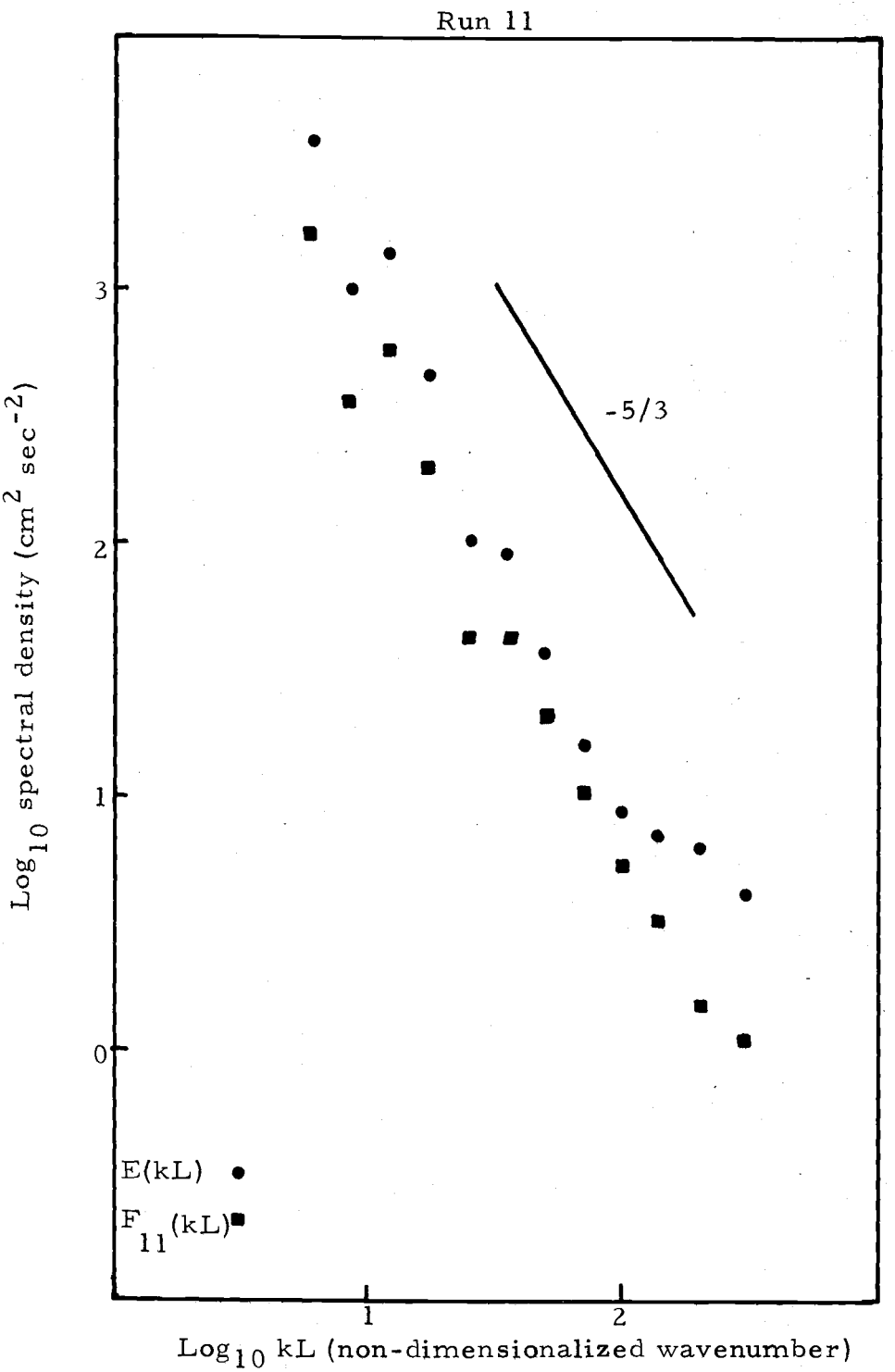

Figure I. Energy spectra.

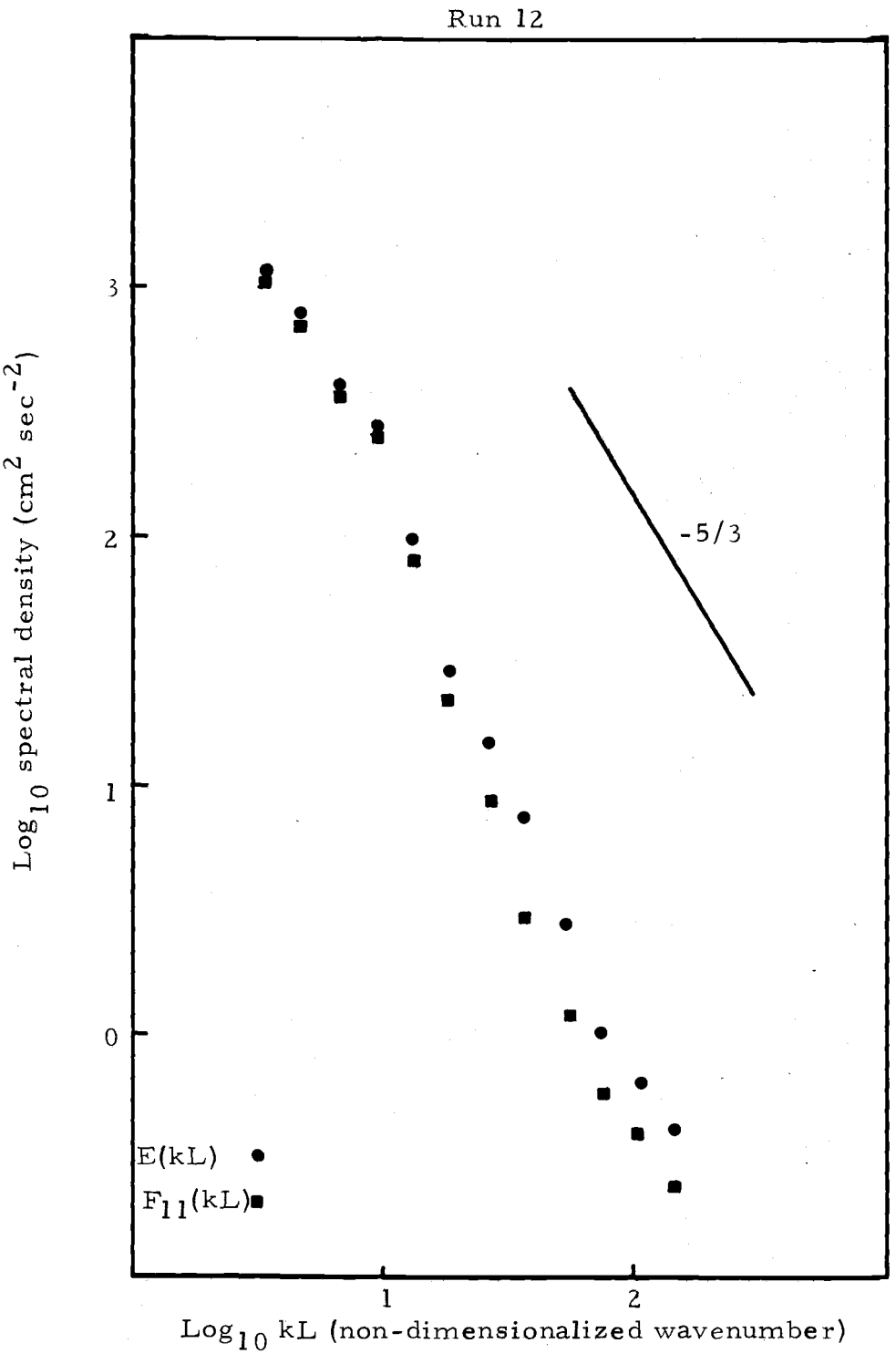

Figure J. Energy spectra.

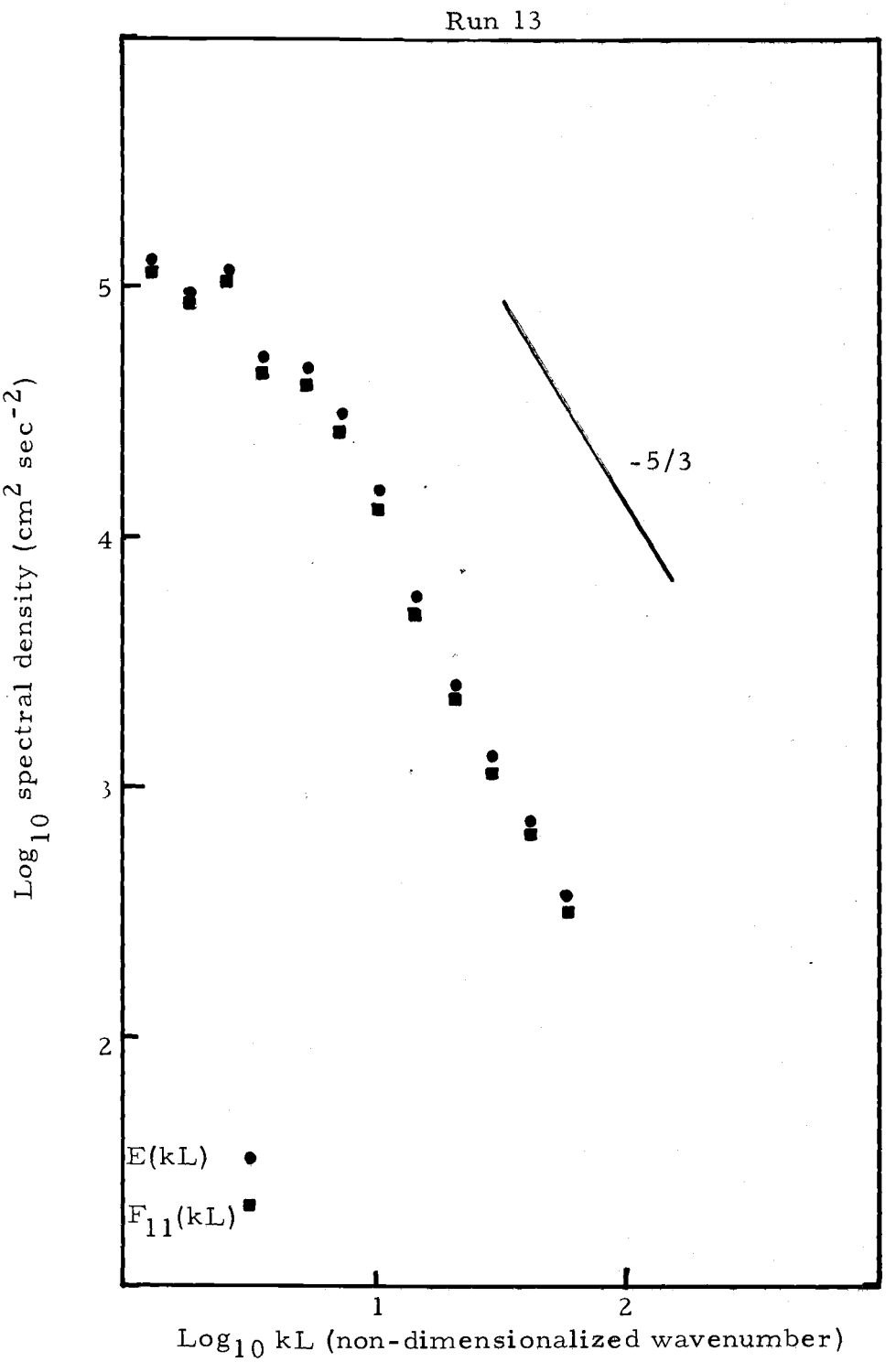

Figure K. Energy spectra.

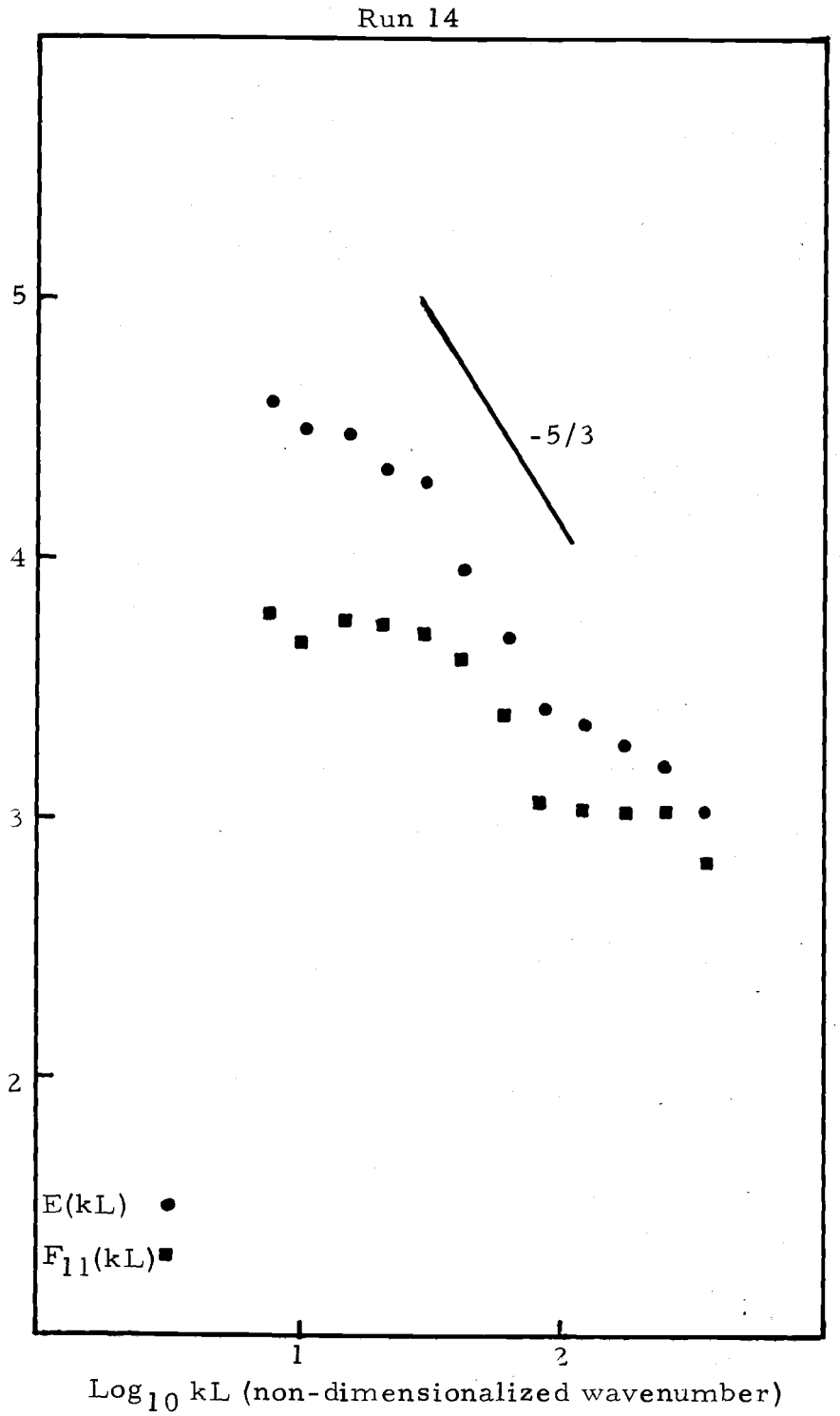

Figure L. Energy spectra.

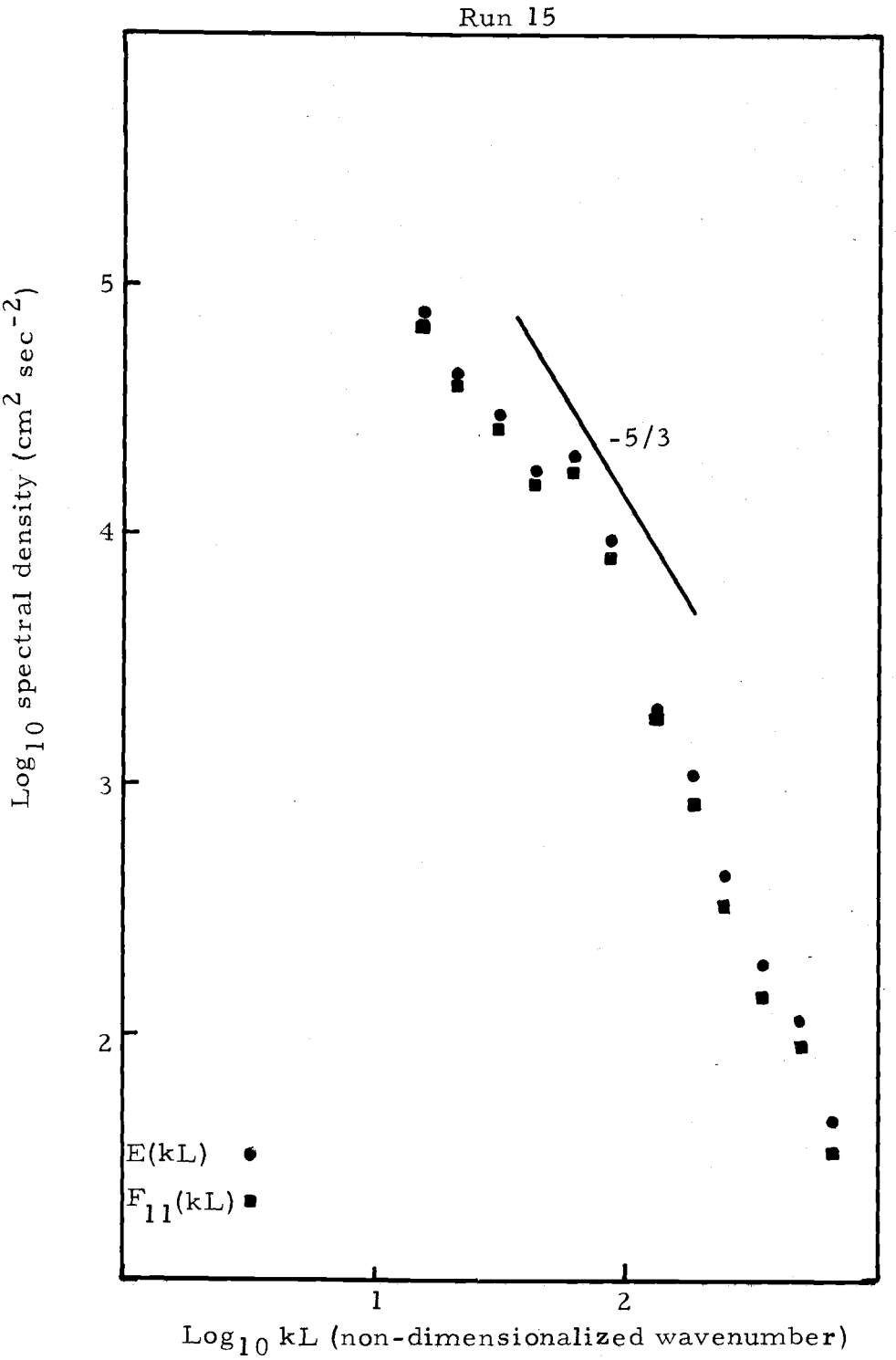

Figure M. Energy spectra.

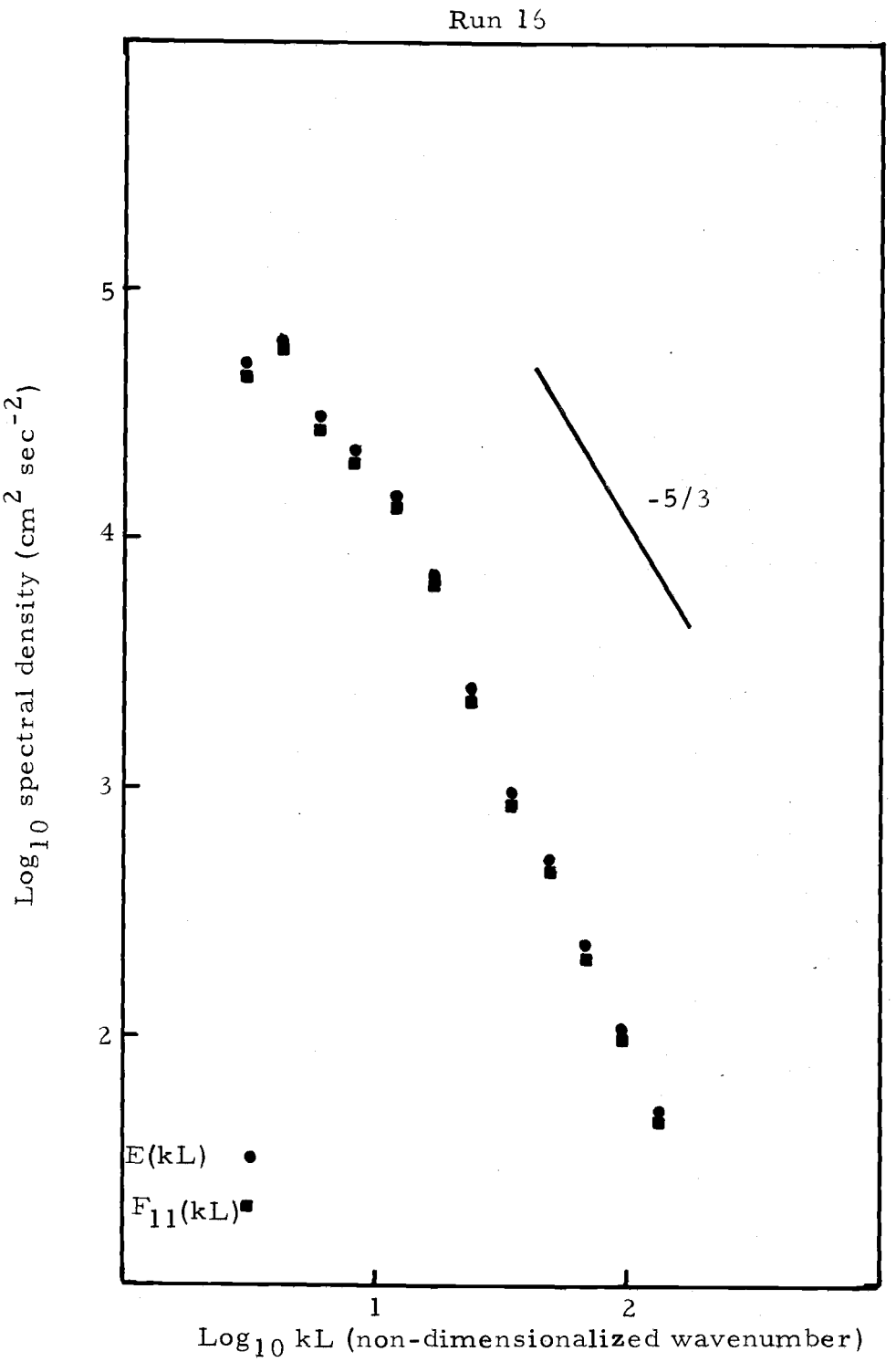

Figure N. Energy spectra.

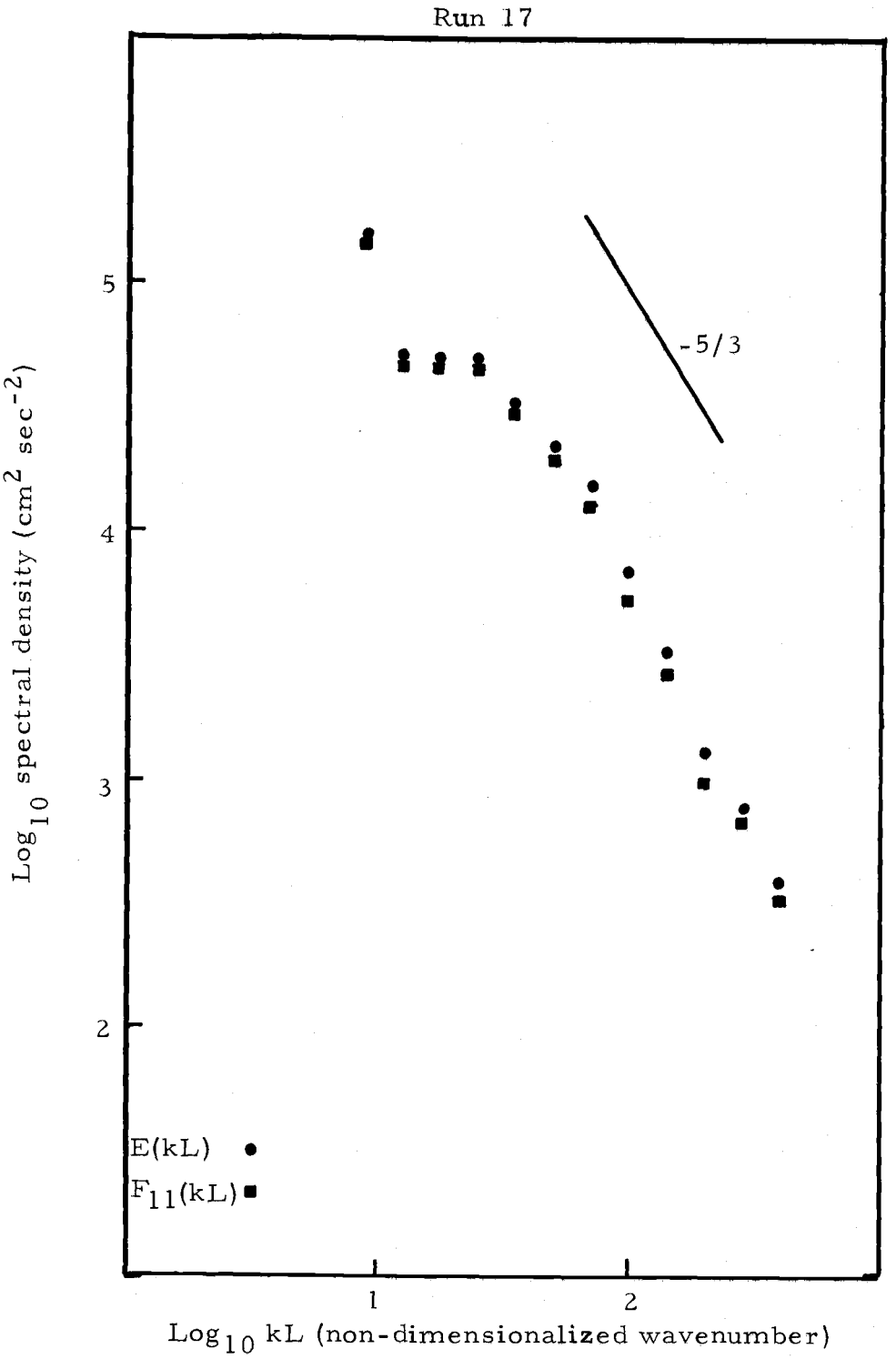

Figure O. Energy spectra.

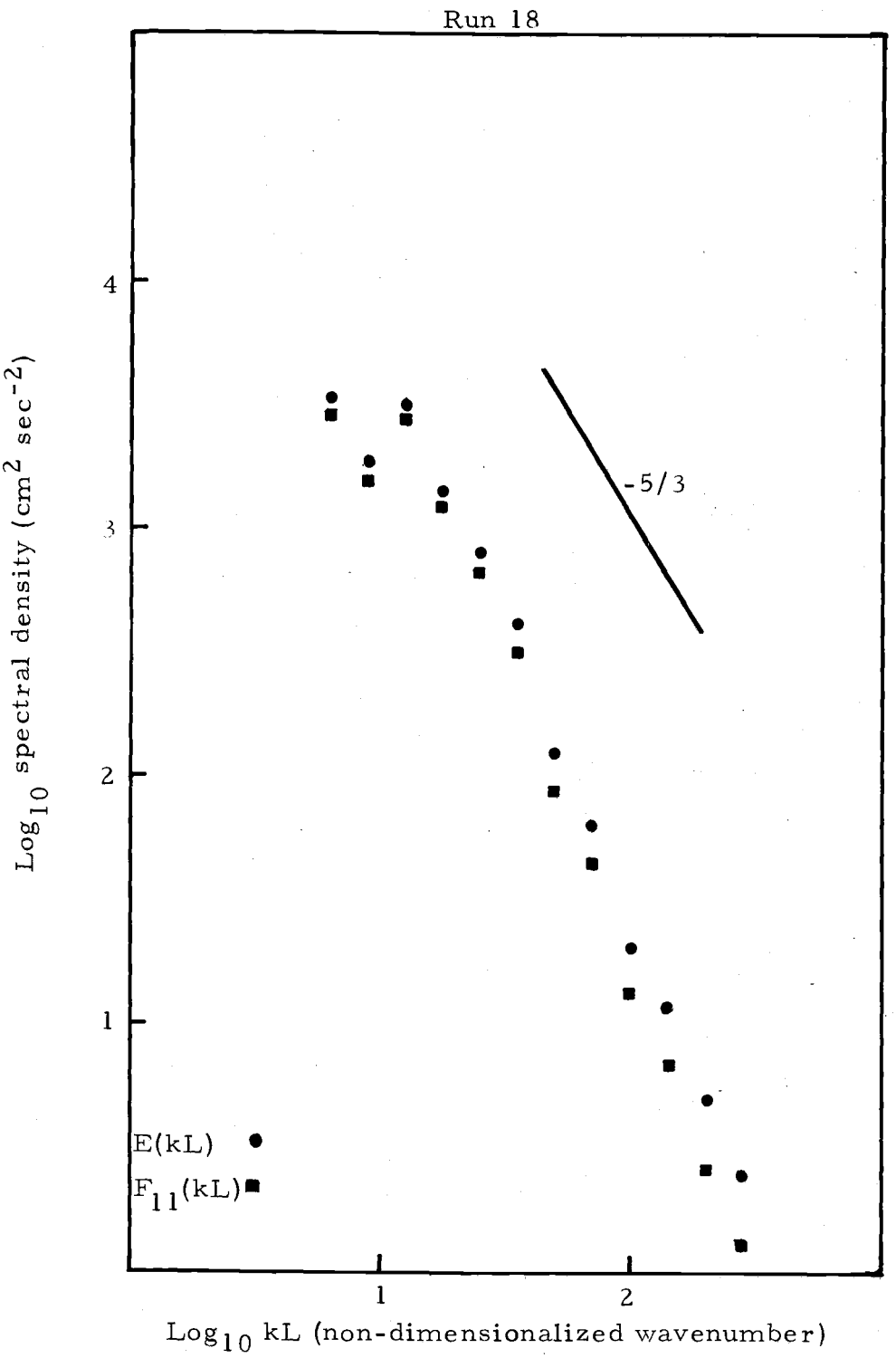

Figure P. Energy spectra.

APPENDIX 3

The stability of a differential equation depends on whether the equation satisfies a Lipschitz condition. For a system of differential equations of the form $u_i' = f_i(u,t)$, if f is differentiable with respect to u and $\partial f/\partial u \leq L$ for some finite L, then the Lipschitz condition is satisfied. Equivalently we can say that if there exists a finite L such that $L = \text{lub } \lambda_i$ where the λ_i are the eigenvalues of the matrix $\partial f_i/\partial u_j$ then L is the Lipschitz constant which will satisfy the Lipschitz condition for the equation. If we rewrite equation (1) in the form $u_i' = f_i(u,t)$ then $f(u,t) = au_i\ u + BF_i(t)$. This implies that $\partial f_i/\partial u_j = (\partial/\partial u_j)(au_i(u_k u_k)^{1/2} + (\partial/\partial u_j)(BF_i(t))$. Letting $u_k u_k = \xi$ and noting that $\partial \xi^{1/2}/\partial u_i = u_i\ \xi^{-1/2}$ we can write in matrix form the following equation:

$$\frac{\partial f_i}{\partial u_j} = a\xi^{-1/2}\begin{bmatrix} \xi + u_1u_1 & u_1u_2 & u_1u_3 \\ u_1u_2 & \xi + u_2u_2 & u_2u_3 \\ u_1u_3 & u_2u_3 & \xi + u_3u_3 \end{bmatrix}$$

The eigenvalues of this equation are the λ_i such that $0 = \det(\partial f_i/\partial u_j - \lambda I)$ where I is the identity matrix. If we let $\gamma = (\xi - \lambda)$ then we can write

$$0 = \det \frac{a}{\xi^{1/2}} \begin{bmatrix} u_1u_1 + \gamma & u_1u_2 & u_1u_3 \\ u_1u_2 & u_2u_2 + \gamma & u_2u_3 \\ u_1u_3 & u_2u_3 & u_3u_3 + \gamma \end{bmatrix}$$

Since a det(A) = det(aA) where a is a scalar and A i a matrix, we can factor out the scalar quantity and evaluate the remaining matrix part. Using Cramer's rule for determinants we can simplify to

$$0 = \gamma^3 + \gamma^2 \xi$$

or equivalently $\gamma = 1$ multiplicity one, $\gamma = 0$ multiplicity two. Since $\gamma = \xi - \lambda$ this implies that $\lambda = \xi$ multiplicity two and $\lambda = 2\xi$ multiplicity one. Thus the eigenvalues of $\partial f_i/\partial u_j$ are $(a|u|, a|u|, 2a|u|)$. This indicates that whenever the magnitude of the velocity ($|u|$) is finite, which it must be in any real physical situation, the equations have a finite Lipschitz constant.

APPENDIX 4

Low Tide

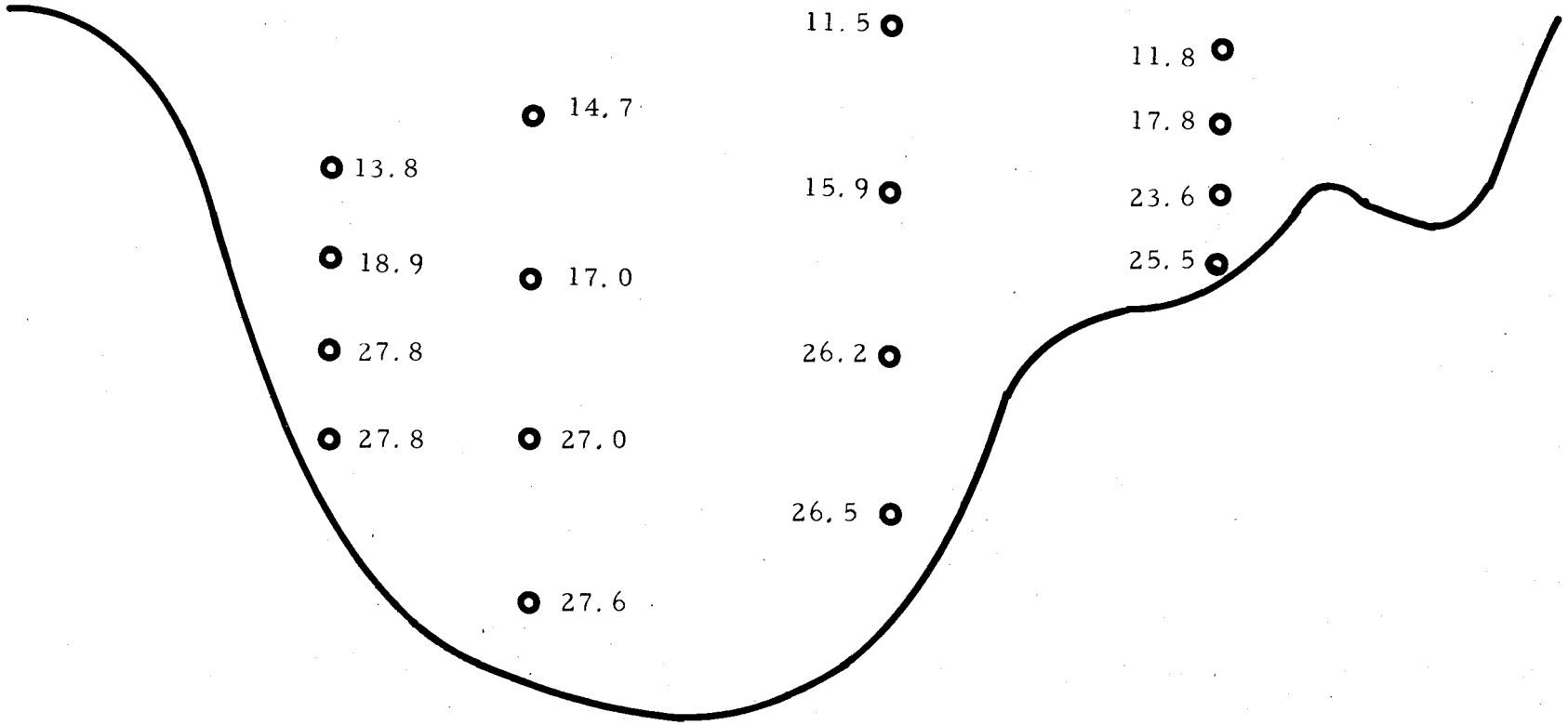

Salinity section across Yaquina Bay

Incoming Tide

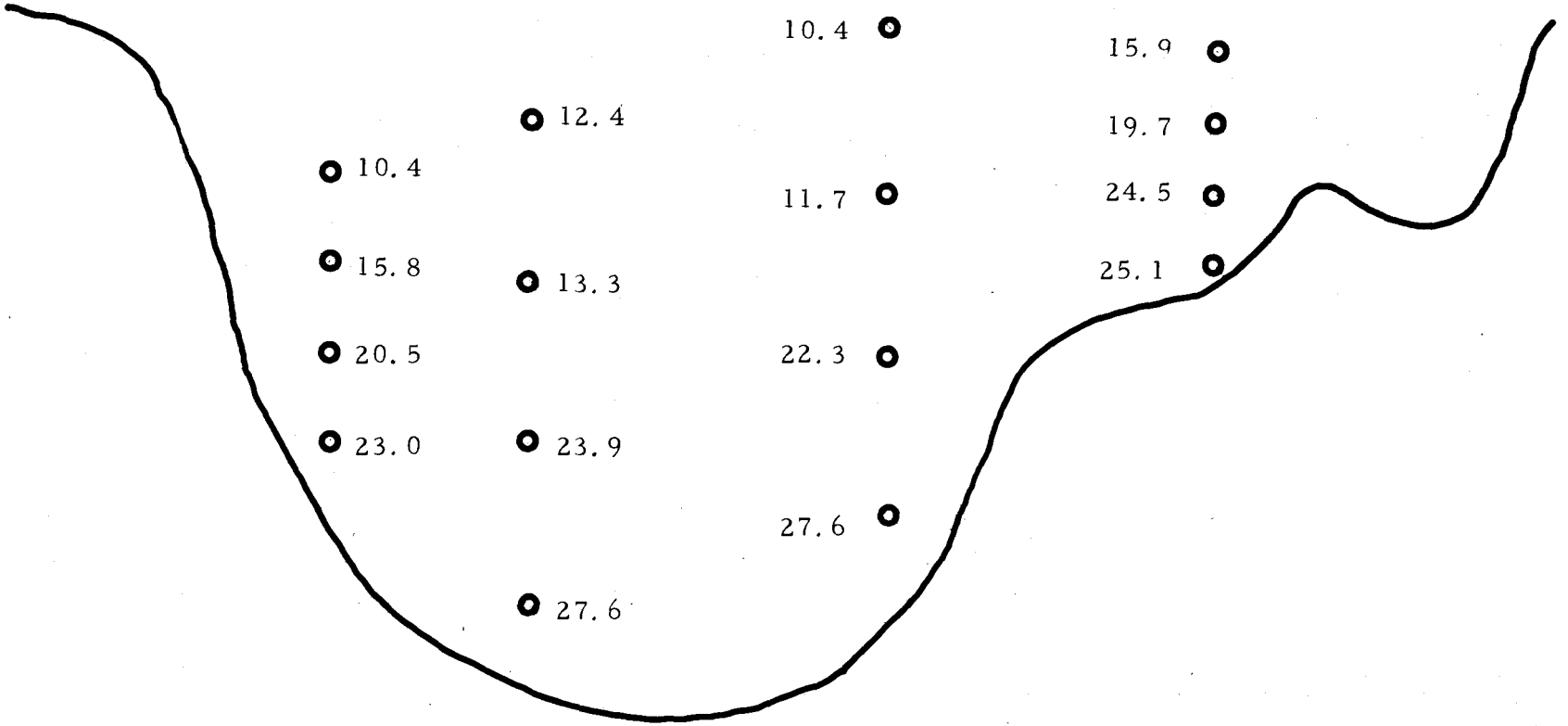

High Tide

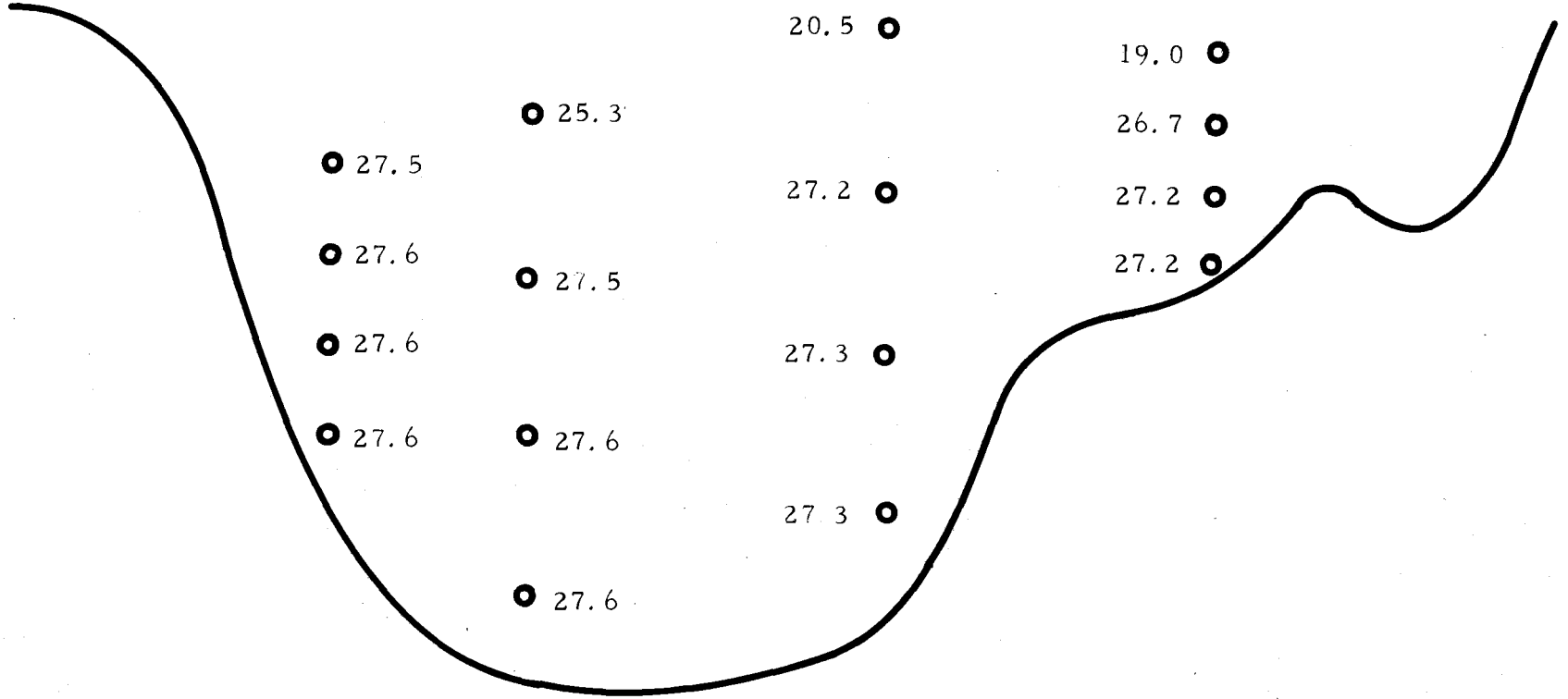

Salinity section across Yaquina Bay